ORIGINAL ARTICLE

CANCER COMMUNICATIONS
Open Access

N6-methyladenosine-modified *DBT* alleviates lipid accumulation and inhibits tumor progression in clear cell renal cell carcinoma through the ANXA2/YAP axis-regulated Hippo pathway

Daojia Miao[1,2,†] | Qi Wang[1,2,†] | Jian Shi[1,2,†] | Qingyang Lv[1,2,†] | Diaoyi Tan[1,2] | Chuanyi Zhao[1,2] | Zhiyong Xiong[1,2] | Xiaoping Zhang[1,2] (ORCID)

[1]Department of Urology, Union Hospital, Tongji Medical College, Huazhong University of Science and Technology, Wuhan, Hubei, P. R. China

[2]Institute of Urology, Union Hospital, Tongji Medical College, Huazhong University of Science and Technology, Wuhan, Hubei, P. R. China

Correspondence
Zhiyong Xiong, Department of Urology, Union Hospital, Tongji Medical College, Huazhong University of Science and Technology, Wuhan 430022, Hubei, P. R. China.
E-mail: tjxiongzhiyong@163.com

Xiaoping Zhang, Department of Urology, Union Hospital, Tongji Medical College, Huazhong University of Science and Technology, Wuhan 430022, Hubei, P. R. China.
E-mail: xzhang@hust.edu.cn

Abstract

Background: The mechanism of metabolism reprogramming is an unsolved problem in clear cell renal cell carcinoma (ccRCC). Recently, it was discovered that the Hippo pathway altered tumor metabolism and promoted tumor progression. Thus, this study aimed at identifying key regulators of metabolism reprogramming and the Hippo pathway in ccRCC and pinpointing potential therapeutic targets for ccRCC patients.

Methods: Hippo-related gene sets and metabolic gene sets were used to screen potential regulators of the Hippo pathway in ccRCC. Public databases and samples from patients were applied to investigate the association of dihydrolipoamide branched chain transacylase E2 (*DBT*) with ccRCC and Hippo signaling. The role of DBT was confirmed by gain or loss of function assays in

vitro and in vivo. Mechanistic results were yielded by luciferase reporter assay,
immunoprecipitation, mass spectroscopy, and mutational studies.

Results: *DBT* was confirmed as a Hippo-related marker with significant prognostic predictive value, and its downregulation was caused by methyltransferase-like-3 (METTL3)-mediated N6-methyladenosine (m^6A) modification in ccRCC. Functional studies specified DBT as a tumor suppressor for inhibiting tumor progression and correcting the lipid metabolism disorder in ccRCC. Mechanistic findings revealed that annexin A2 (ANXA2) interacted with the lipoyl-binding domain of DBT to activate Hippo signaling which led to decreased nuclear localization of yes1-associated transcriptional regulator (YAP) and transcriptional repression of lipogenic genes.

Conclusions: This study demonstrated a tumor-suppressive role for the DBT/ANXA2/YAP axis-regulated Hippo signaling and suggested DBT as a potential target for pharmaceutical intervention in ccRCC.

KEYWORDS
clear cell renal cell carcinoma, lipid accumulation, Hippo signaling, N6-methyladenosine,
dihydrolipoamide branched chain transacylase E2

1 | BACKGROUND

Renal cell carcinoma (RCC) is a common malignancy of the urinary system, accounting for approximately 90% of kidney cancers [1]. Clear cell renal cell carcinoma (ccRCC) is the dominant pathological subtype of RCC, representing about 70% of RCC [2]. ccRCC may be easily misdiagnosed due to its insidious onset and lack of specific clinical symptoms in the early stage [3]. Currently, ccRCC treatment is mainly based on a combination of surgery and targeted drugs [4]. However, the difficulty of early diagnosis, the tolerance of targeted drugs and the huge fluctuation of patient survival rate are the challenges in managing ccRCC [3, 4]. Therefore, investigating ccRCC pathogenesis and exploring new treatments for ccRCC patients have become the hotspot of current cancer research.

Metabolic reprogramming is a prevalently and physiologically vital change in many types of cancer [5–7]. Tumors gradually adapt metabolically to various extracellular and intracellular stimuli as they progress [6]. ccRCC has marked metabolic abnormalities and was once considered a metabolism-related disease [7, 8]. The most significant metabolic abnormalities in ccRCC are lipid metabolism abnormalities, which lead to the abundance of lipid droplets in the cytoplasm [9]. Nonetheless, there have been few systematic studies on lipid metabolism in ccRCC. Until recently, scholars gradually recognized the importance of lipid metabolism in the development of ccRCC. Research has revealed that lipid droplets in ccRCC reduced the endoplasmic reticulum stress and enhanced cell

viability, thereby promoting ccRCC [10]. Therefore, a better understanding of the molecular mechanisms underlying lipid accumulation in ccRCC is required.

Genetic studies in Drosophila melanogaster define the Hippo pathway as an evolutionarily conserved controller of organ size [11–13]. Briefly, Hippo signaling is activated by a kinase signaling cascade and subsequently leads to transcriptional inactivation of target genes which play a remarkable role in tissue homeostasis and organ development [14]. Recently, the relationship between the dysregulation of the Hippo pathway and carcinogenesis has garnered attention [15]. New studies on cancers coupled lipid metabolism to the Hippo pathway [16] and suggested that lipid accumulation is accelerated by yes1-associated transcriptional regulator (*YAP*) activation [16, 17], which then upregulated the expression of lipogenic genes [18]. It has been reported that when Hippo signaling was turned off, it promoted tumor initiation, progression and metastasis in various cancers [19]. Furthermore, emerging evidence demonstrates that the dysfunction of the Hippo pathway contributes to the development of ccRCC [20, 21]. Therefore, it necessitates exploring the relationship between the Hippo pathway and lipid metabolism in ccRCC.

Dihydrolipoamide branched chain transacylase E2 (DBT) is the core component of branched-chain alpha-keto acid dehydrogenase complex [22]. DBT was involved in the metabolism of branched-chain amino acids, and its mutation has been shown to cause maple syrup urine disease [23]. Also, it has been stated that DBT interacts

with different proteins and functions in the context of complexes [22, 24-26]. For example, renal oxidative stress could increase the interaction between DBT and peroxiredoxin V as well as the enzymatic activity of DBT [25]. A previous study signified that DBT was associated with Hippo signaling due to its interaction with YAP [26]. However, the role of DBT in tumors, particularly in ccRCC, is largely undefined and under-reported.

In the present study, we evaluated the expression level and the prognostic value of *DBT* in ccRCC. Then in vitro and in vivo assays were used to validate the function of DBT in ccRCC. Moreover, the mechanism underlying DBT-regulated ccRCC progression was carefully explored.

2 | METHODS AND MATERIALS

2.1 | Tissue samples and cell lines

Human ccRCC tissues and adjacent normal tissues were acquired from 24 patients in the Department of Urology, Wuhan Union Hospital (Wuhan, Hubei, China). The 8th edition of American Joint Committee on Cancer TNM Staging was used for tumor staging. The following were the inclusion criteria: 1) all patients underwent partial or total nephrectomy for ccRCC; 2) all patients were pathologically diagnosed with ccRCC between June 2019 and June 2021. The exclusion criteria included: 1) patients with two or more primary malignancies; 2) patients with incomplete clinical information. All patients had written informed consent, and this study was approved by the Institutional Review Board of Huazhong University of Science and Technology (IEC-072).

Human ccRCC cell lines A498, 786-O, CAKI-1, and OSRC-2 were obtained from the American Type Culture Collection (ATCC, Manassas, VA, USA). Human embryonic kidney cell lines HEK293 and HEK293T were also obtained from the ATCC. Cell lines used in the present study were validated by short tandem repeat profiling on Aug 14, 2021. Cells were cultured in Dulbecco's modified eagle medium (DMEM, Gibco, Waltham, MA, USA) containing 10% fetal bovine serum (Gibco) at 37°C in 5% CO_2.

2.2 | Real-time PCR

The Magzol reagent (#R4801, Magen, Guangzhou, Guangdong, China) was applied for RNA isolation with the guidance of the manufacturer's protocols. Reverse transcription-PCR (RT-PCR) was conducted and normalized to glyceraldehyde-3-phosphate dehydrogenase (*GAPDH*). Briefly, total RNA (500 ng) from cells and tissues was reversely transcribed into complementary DNA (cDNA), and quantitative PCR (qPCR) was conducted (qTOWER, Analytik Jena, Jena, Germany) with the Sybr Green Mix (#11203ES03, Yeasen, Shanghai, China). The followings were the thermal cycling conditions: 5 min at 95°C, 42 cycles of 15 s at 95°C, 30 s at 60°C. Primer sequences are provided in Supplementary Table S1.

2.3 | Methylated RNA immunoprecipitation (MeRIP)-qPCR

Total RNA was extracted from tissue samples and ccRCC cells by the Magzol Reagent. Polyadenylated RNA was isolated from total RNA using the mRNA library prep kit (#12301ES24, Yeasen). RNA fragmentation reagents (#12301ES24, Yeasen) were used to randomly fragment RNA. The N6-methyladenosine (m^6A) antibody was applied for MeRIP. Both the input group and MeRIP group were prepared for gene-specific m^6A qPCR. Briefly, 4 µg mRNA was equally divided into the input group and MeRIP group. As for the MeRIP group, 2 µg mRNA was incubated with m^6A antibody and diluted into 500 µL MeRIP buffer supplemented with 100 U RNase inhibitor (#R0102, Beyotime, Shanghai, China). Then magnetic beads (#HY-K0202, MedChemExpress, Monmouth Junction, NJ, USA) were added to the mixture and rotated at 4°C for 12 h. After 4 times washing by MeRIP buffer, the MeRIP portion was used to extract MeRIP mRNA by Magzol and ethanol precipitation. Then RT-qPCR was conducted by using MaterMix and SuperMix (Vazyme, Nanjing, Jiangsu, China) from MeRIP mRNA and Input mRNA. The relative mRNA expression was evaluated by the number of amplification cycles (Cq). More detailed experimental methods were described in a previous study [27]. The following is the calculation formula:

$$\Delta Cq_{(Control)} = Cq_{(MeRIP)} - Cq_{(Input)};$$

$$\Delta Cq_{(Treatment)} = Cq_{(MeRIP)} - Cq_{(Input)};$$

Relative m^6A modification level $= 2^{\Delta CT(Control) - \Delta CT(Treatment)}$.

2.4 | mRNA stability assays

Cells were seeded into 6-well plates at a density of 50% confluency and cultured for 24 h. Dimethyl sulfoxide (DMSO, Aladdin, Shanghai, China) was used in the control group, and 5 µg/mL actinomycin D (#HY-17559, MedChemExpress) was used in the treatment group. After cells were treated with DMSO or actinomycin D for 0, 2, 4, 6, 8, or 12 h, they were collected to extract total RNA. Next, RT-qPCR assays were conducted, and the half-life of mRNA was calculated based on the Cq value. More details

of mRNA stability assays were described in a previous study [28].

2.5 | Western blotting

Radio-immunoprecipitation assay protein lysis buffer (#P0013C, Beyotime) supplemented with phenylmethane-sulfonylfluoride (#ST506, Beyotime) and protease inhibitor cocktail (#P1005, Beyotime) was used to extract protein from tissues and ccRCC cells. The total protein (30 μg) was electrophoresed on sodium dodecyl sulfate-polyacrylamide gel. Then, proteins were transferred to polyvinylidene fluoride membranes (Roche, Basel, Switzerland). The primary antibodies were used to decorate the membranes and incubated in the blocking buffer with secondary antibodies for 2 h before detection. The list of antibodies used in this study is provided in Supplementary Table S2.

2.6 | Cycloheximide chase assays

Cells were treated with 50 μmol/L cycloheximide (#HY-12320, MedChemExpress) for 0, 8, 16 and 24 h. Cells were harvested for Western blotting analysis. ImageJ software (National Institutes of Health, Bethesda, MD, USA) was used to quantitatively analyze protein levels in Western blotting assays.

2.7 | Cell transfection and infection

Small interfering RNAs (siRNA) (Supplementary Table S3) were synthesized by Genepharma (Shanghai, China) and transfected into cells by Lipofectamine 6000 (#C0526, Beyotime). Lentiviruses of Flag-DBT and annexin A2 (ANXA2) short hairpin RNA (shRNA) (Supplementary Table S3) were purchased from Genechem (Shanghai, China) and then infected A498 and CAKI-1 cells with the guidance of the manufacturer's protocols. The human methyltransferase-like-3 (METTL3) and Myc-ANXA2 were cloned into the GM19315-lenti-CMV-MCS-PGK-Puro vector (Genomeditech, Shanghai, China) to construct over-expression plasmids. Cell lysates and total RNA were collected at 72 h after the transfection or the infection to verify their efficiency by Western blotting and qPCR.

2.8 | Dual-luciferase reporter assays

Following the instruction of the dual-luciferase reporter assay system (Promega, Madison, WI, USA), cells were seeded at 70%-80% confluency in 6-well plates and then transfected with a Dual-luciferase reporter vector fused to the wild-type (WT) or mutated (MUT) 3′-untranslated regions (UTR). METTL3 or empty vectors were also transfected into HEK293T cells. Renilla luciferase activity was regarded as an internal reference. The fluorescence signal was detected by a multimode plate reader (EnSpire, Perkin Elmer, Waltham, MA, USA).

2.9 | Cell viability assays

Cells were seeded in a 96-well plate at a density of 2000 cells/well. Cell counting kits (CCK8, Yeasen) were applied to detect the proliferation rate of cells. The CCK8 solution (10 μL) mixed with 100 μL DMEM was added to each well, and the plate was incubated in dark at 37°C. The optical density value at 450 nm was measured at 0, 24, 48, 72 and 96 h by spectrophotometer (NanoDrop Technologies, Wilmington, DE, USA). The doubling time of cells was calculated using the following equation: Duration × [lg 2 / (lg (final concentration / initial concentration)] [29].

2.10 | Colony formation assays

Briefly, cells were plated in 6-well plates at 1000 cells/well. Two weeks later, cells were washed with phosphate-buffered saline (PBS), fixed with methanol, and stained with 0.05% crystal violet (#G1014, Servicebio, Wuhan, Hubei, China). The photographs of colonies growing on the plates were taken on day 14. The colony formation rate (%) = (number of colony / number of seeded cells) × 100%.

2.11 | Transwell assays

The procedure was carried out as previously described [30]. Cells were starved for 24 h. The top chamber of the Transwell plate (#REF3422, Corning Inc., Corning, NY, USA) was coated by the Matrigel (#356234, dilution 1:8, Corning Inc.). Then cells were plated in the top chamber at a density of 10^5 cells/chamber. After 24 h, cells that had invaded the lower surface of the chamber membrane were fixed by methanol. Next, cells stained with 0.05% crystal violet were randomly photographed. Additionally, Transwell chambers that were not coated by the Matrigel were used to examine the migration ability of ccRCC cells.

2.12 | Animal models

Five-week-old male BALB/c nude mice were obtained from Vital River Laboratories (Beijing, China) and housed in a specific pathogen-free environment. All animal

studies were approved by the Institutional Animal Use and Care Committee of Tongji Medical College (S1892).

Subcutaneous tumor models were established by subcutaneous injection of a total of 2×10^6 tumor cells in nude mice ($n = 5$). Subcutaneous tumors were measured every 4 days. Mice were euthanized by CO_2 and cervical dislocation on day 44 or when the tumor size exceeded 1.5 cm in diameter, and the tumors were dissected, photographed, and weighed.

Metastatic tumor models were established through tail vein injection of 4×10^6 tumor cells in nude mice ($n = 3$) to evaluate the metastatic ability of tumor cells. After 8 weeks, nude mice were used for live small animal fluorescent imaging assays by the LagoX system (Spectral instruments imaging, Tucson, AZ, USA).

2.13 | Immunohistochemistry (IHC)

IHC was performed on tissues from patients and subcutaneous tumor models. The detailed procedures were described in our previous study [31]. Briefly, after being fixed by 4% paraformaldehyde, tissues were sequentially dehydrated, embedded in paraffin, sectioned, deparaffinized, and rehydrated for antigen retrieval. Then the tissue sections were blocked in bovine serum albumin and incubated with primary antibodies and corresponding secondary antibodies. The microscope (#DSZ2000, UOP Photoelectric Technology, Chongqing, China) was used to randomly photograph the sections. The antibodies used in IHC are provided in Supplementary Table S2. Semiquantitative analysis of IHC was carried out by three experienced pathologists according to the following criteria: IHC score = the staining intensity of the interested protein (0 = negative staining; 1 = weak staining; 2 = moderate staining; 3 = strong staining) × percentage of positive cells (0 = 0%; 1 = 1%-25%; 2 = 26%-50%; 3 = 51%-75%; 4 = 76%-100%). The optimal cut-off value of DBT generated from the receiver operating characteristic (ROC) curves divided DBT protein expression into the high or low group. All patients had written informed consent for the use of their tissue samples in this study.

2.14 | Oil red staining

Cells plated at 30%-40% confluency in 12-well plates were fixed with 4% paraformaldehyde for 15 min. They were then rinsed with PBS twice for 10 min, stained with Oil red (#G1015, Servicebio) for 15 min, and washed with water three times. Then, the 12-well plate was randomly photographed with a microscope (#DSZ2000, UOP Photoelectric Technology).

2.15 | Triglyceride (TG) detection

Cells were plated at 50% confluency in a 6 cm dish. After being cultured for 24 h, the cell pellet was collected from the 6 cm dish. After adding 0.9 mL of Triton X-100 (#P0096, Beyotime), 0.1 g of subcutaneous tumor or cell pellet from the 6 cm dish was mechanically homogenized and centrifuged at 600 ×g for 10 min. The supernatant was then used to detect the content of TG following the instruction of the Triglyceride assay kit (#A110-1-1, Jiancheng, Nanjing, Jiangsu, China).

2.16 | Flow cytometry apoptosis assay

Cells were harvested to analyze cell apoptosis by flow cytometry (Becton Dickinson, Franklin Lakes, NJ, USA) after being stained with Annexin V-Phycoerythrin (PE) and 7-amino-actinomycin D (7-AAD) (#A213-01, Vazyme). Different combinations of 7-AAD and PE can identify apoptosis at different stages. The results were analyzed with FlowJo software (Becton Dickinson).

2.17 | Immunofluorescence

Cells were plated on the round coverslip (Biosharp, Hefei, Anhui, China) at a density of 10^5 cells/coverslip. After washing with PBS, cells were fixed with 4% formaldehyde for 10 min, permeabilized with 0.5% Triton X-100 for another 10 min and blocked with 5% bovine serum albumin. The coverslips were then incubated with primary antibodies at 4°C overnight and Alexa Fluor 594-conjugated goat anti-rabbit IgG (#AS039, dilution 1:250, ABclonal, Wuhan, Hubei, China) at room temperature for 2 h. Nuclei were stained with 4',6-diamidino-2-phenylindole (DAPI) solution (#C1002, Beyotime) at room temperature for 15 min, and the images were captured by a DMI3000B fluorescence microscope (Leica, Wetzlar, Hessen, Germany).

2.18 | Subcellular fractionation

Cytosolic and membrane fractions of ccRCC cells were obtained by using the membrane and cytosol protein extraction kit (#P0033, Beyotime) according to the manufacturer's protocol. Cytoplasmic and nuclear fractions of ccRCC cells were performed by the nuclear and cytoplasmic protein extraction kit (#P0028, Beyotime) by following the manufacturer's protocol.

2.19 | RNA-sequencing (RNA-seq) analysis

RNA samples were isolated from paired ccRCC and adjacent normal tissues from 3 patients using Magzol Reagent or extracted from the products of MeRIP. Then RNA samples were qualified and quantified for mRNA purification. After being fragmented by divalent cations, mRNA was amplified by PCR. The products from PCR were used for library construction. Finally, the sequencing library was sequenced on DNBSEQ-T7 (Making Great Innovation, Shenzhen, Guangdong, China) with the PE150 model according to the manufacturer's protocol. Techniques and methods for whole-transcriptome sequencing were provided by Bioyi Biotechnology Co., Ltd. (Wuhan, Hubei, China).

2.20 | Co-immunoprecipitation (co-IP)

The cell lysate extracted from ccRCC cells was incubated in co-IP buffer (#HY-K0202, MedChemExpress) with primary antibodies or IgG overnight at 4°C with shaking. The immune complexes were incubated with protein A/G magnetic beads for 2 h at room temperature followed by washing with PBST (PBS + 0.05% Tween 20) to remove the unbound immune complexes. The bound immune complexes dissociated from the beads were used for Western blotting assays.

2.21 | Mass spectrometry (MS) analysis

The MS analysis was performed by the GeneCreate Biological Engineering Co., Ltd (Wuhan, Hubei, China). Briefly, the magnetic immune complexes from co-IP assays were electrophoresed to obtain gel strips. Then, protein gel strips were sequentially decolorized, alkylated, enzymatically hydrolyzed, extracted, and desalted into peptide samples. Then the peptide samples were analyzed by the Triple TOF 5600 + LC/MS system (AB SCIEX, Framingham, MA, USA). Finally, the original MS/MS files from the mass spectrometer were submitted to ProteinPilot (Version 4.5, SCIEX, Redwood, CA, USA) for data analysis. For protein identification, the Paragon algorithm in ProteinPilot was used to search the Uniprot database (https://www.uniprot.org/). Peptides with an unused score > 1.3 (a credibility of more than 95%) were considered credible peptides, and proteins containing at least one unique peptide are retained.

2.22 | Bioinformatics and statistical analyses

The list of proteins that interact with YAP was downloaded from the study by Hauri et al. [26]. Public RNA-seq data were downloaded from the Oncomine database (https://www.oncomine.org), the cancer genome atlas (TCGA) repository (https://portal.gdc.cancer.gov), and the Gene expression omnibus (GEO) database (GSE6344, https://www.ncbi.nlm.nih.gov/gds). Pearson correlation coefficient analyses were applied to validate the correlations between *DBT* and the components of the Hippo pathway at the mRNA level, and $P < 0.05$ meant the data were statistically significant. Differentially expressed genes (DEGs) were identified using the 'DESeq2' package in the software R (R Core Team, https://www.r-project.org). The criteria used to define DEGs were set as adjusted $P < 0.05$ and |log fold-change| >1.5. Functional enrichment analysis was performed by Gene set enrichment analysis (GSEA) and Kyoto encyclopedia of genes and genomes (KEGG) analysis. ROC analyses were applied to assess the clinical diagnostic value. Kaplan-Meier analyses were applied to compare the survival distributions of the high or low *DBT* expression groups with the log-rank test. The overall survival was calculated from the initial pathologic diagnosis of ccRCC to death from any cause or the most recent follow-up. Prognostic factors were examined by univariate and multivariate Cox regression. The α levels of univariate and multivariate Cox regression were set as the followings: α (entry) = 0.05 and α (removal) = 0.1. Additionally, the sequence-based m^6A modification site predictor (SRAMP, http://www.cuilab.cn/sramp) was used to predict the potential m^6A modification site based on the cDNA sequence of *DBT*. Intropro (http://www.ebi.ac.uk/interpro/about.html) was used to identify domains based on the amino acid sequence of *DBT*. Statistical analysis was conducted using Excel 2019 (Microsoft, Redmond, WA, USA) and SPSS 26.0 (IBM Corporation, Armonk, NY, USA). Data are presented as the mean ± standard deviation and analyzed using Student's *t*-test, analysis of variance (ANOVA), and nonlinear regression. Assays in this study were performed independently at least three times.

3 | RESULTS

3.1 | *DBT* was downregulated in ccRCC and indicated a poor prognosis

The Hippo pathway has recently been linked to tumorigenesis by its eminent roles in cell proliferation, metastasis,

and cancer metabolism [32–34]. A previous study showed that RCC had the largest number of differentially expressed Hippo-related genes, indicating a marked dysregulation of Hippo signaling in RCC [35]. Thus, we performed RNA-seq analyses on three pairs of ccRCC tissues and adjacent normal tissues to explore whether Hippo signaling was dysregulated in ccRCC. It was found that several components in the Hippo pathway had different mRNA levels between ccRCC and adjacent normal tissues (Figure 1A). Furthermore, functional enrichment analyses were performed on 1451 DEGs that were differentially expressed between ccRCC and adjacent normal tissues based on our RNA-seq data. It was noted that the Hippo pathway was enriched in KEGG analysis (Supplementary Figure S1A). Thus, RNA-seq data from the Oncomine database were applied to screen potential regulators of the Hippo pathway in ccRCC. Four candidates involved in the metabolism pathway were selected since their expression levels were significantly correlated to the core component of the Hippo pathway (Figure 1B). The prognostic values of these candidates were evaluated by using the TCGA-kidney renal clear cell carcinoma (KIRC) dataset. Kaplan-Meier analysis showed that low levels of *DBT*, galactokinase 2 (*GALK2*) and succinate-CoA ligase ADP-forming subunit beta (*SUCLA2*) predicted lower survival rates of ccRCC patients (Supplementary Figure S1B). Next, the results of ROC analysis illustrated that among these candidates, *DBT* presented the strongest ability to distinguish between ccRCC patients and healthy individuals because of its biggest area under curve (AUC) (Supplementary Figure S1C). Multivariate Cox regression analyses denoted that high expression of *DBT* was a favorable prognostic factor for ccRCC patients even when adjusted for known risk factors (Table 1). Compared with *SUCLA2*, *GALK* and serine racemase (*SRR*), *DBT* had the most powerful prognostic prediction ability of ccRCC (Supplementary Figure S1D). Furthermore, the functional enrichment analysis showed that DBT was involved in the Hippo pathway (Figure 1C), which verified the screening for Hippo signaling regulator. Thus, this study identified DBT as a potential molecule functioning in ccRCC to regulate the Hippo pathway. Subsequently, it was found that *DBT* was downregulated in ccRCC based on RNA-seq data from GEO (GSE6344) and TCGA-KIRC (Figure 1D). Meanwhile, the expression level of *DBT* was not associated with the gender or age of ccRCC patients (Supplementary Figure S1E). However, the expression level of *DBT* was negatively related to pathological grade and clinical stage (Supplementary Figure S1F). Then, the downregulated mRNA (Figure 1E) and protein levels of *DBT* (Figure 1F) were corroborated in common ccRCC cell lines. Also, it was presented that ccRCC tissues had a lower expression of *DBT* than adjacent normal tissues (Figure 1G-I). IHC assays revealed decreased expression of DBT in ccRCC tissues compared with normal tissues (Figure 1J-K). Altogether, these results confirmed *DBT* downregulation as a predictor of poor prognosis in ccRCC.

3.2 | METTL3-mediated m⁶A modification was involved in *DBT* downregulation

m^{6}A is the most important RNA modification that participates in maintaining cancer malignant phenotype by governing the expression of cancer-related genes [36]. We hypothesized that the mRNA of *DBT* was modified by m^{6}A regulators, such as the methyltransferase complex. The results of MeRIP-qPCR assays showed a stronger enrichment of m^{6}A-modified *DBT* in A498 and CAKI-1 cells than that in HEK293 cells (Figure 2A). It was also noticed that *DBT* possessed higher m^{6}A modification in tumors than in adjacent normal tissues (Supplementary Figure S2A). SRAMP prediction based on the cDNA sequence of *DBT* revealed that six m^{6}A sites were possibly methylated (Figure 2B and Supplementary Table S4). Next, we found that m^{6}A modification levels of *DBT* were increased in the 3′-UTR of tumor cells and tissues (Figure 2C and Supplementary Figure S2B), which was coincident with the notion that a majority of m^{6}A residues displayed a 3′-UTR localization bias and were related to mRNA destabilization [37]. Given that METTL3 is the core component of m^{6}A modification in cancer cells [38], we assessed its expression in ccRCC using data from the TCGA-KIRC database and clinical samples. Notably, METTL3 was upregulated in ccRCC tumors, while *DBT* was downregulated in ccRCC tumors (Figure 2D-E). Then METTL3 was knocked down and overexpressed in A498 and CAKI-1 cells. The results of mRNA stability assays showed that METTL3 reduction enhanced the stability of *DBT* and the reintroduction of METTL3 contributed to a decreased half-life of *DBT* at the mRNA level (Figure 2F and Supplementary Figure S2C). Subsequently, Western blotting and qPCR assays showed that METTL3 reduction caused the increased *DBT* mRNA (Figure 2G) and protein levels (Supplementary Figure S2D). On the contrary, the reintroduction of METTL3 contributed to the decreased mRNA (Figure 2H) and protein levels of DBT (Supplementary Figure S2E). Upon these findings, mutant *DBT* 3′-UTR plasmids were constructed for the luciferase reporter assay to verify its interaction with METTL3 (Figure 2I). The results of luciferase reporter assays showed that METTL3 restrained *DBT* expression through site 1672 rather than site 1653 in the 3′-UTR of *DBT* (Figure 2J). These results denoted the METTL3-mediated m^{6}A methylation reduced the expression of *DBT* in ccRCC.
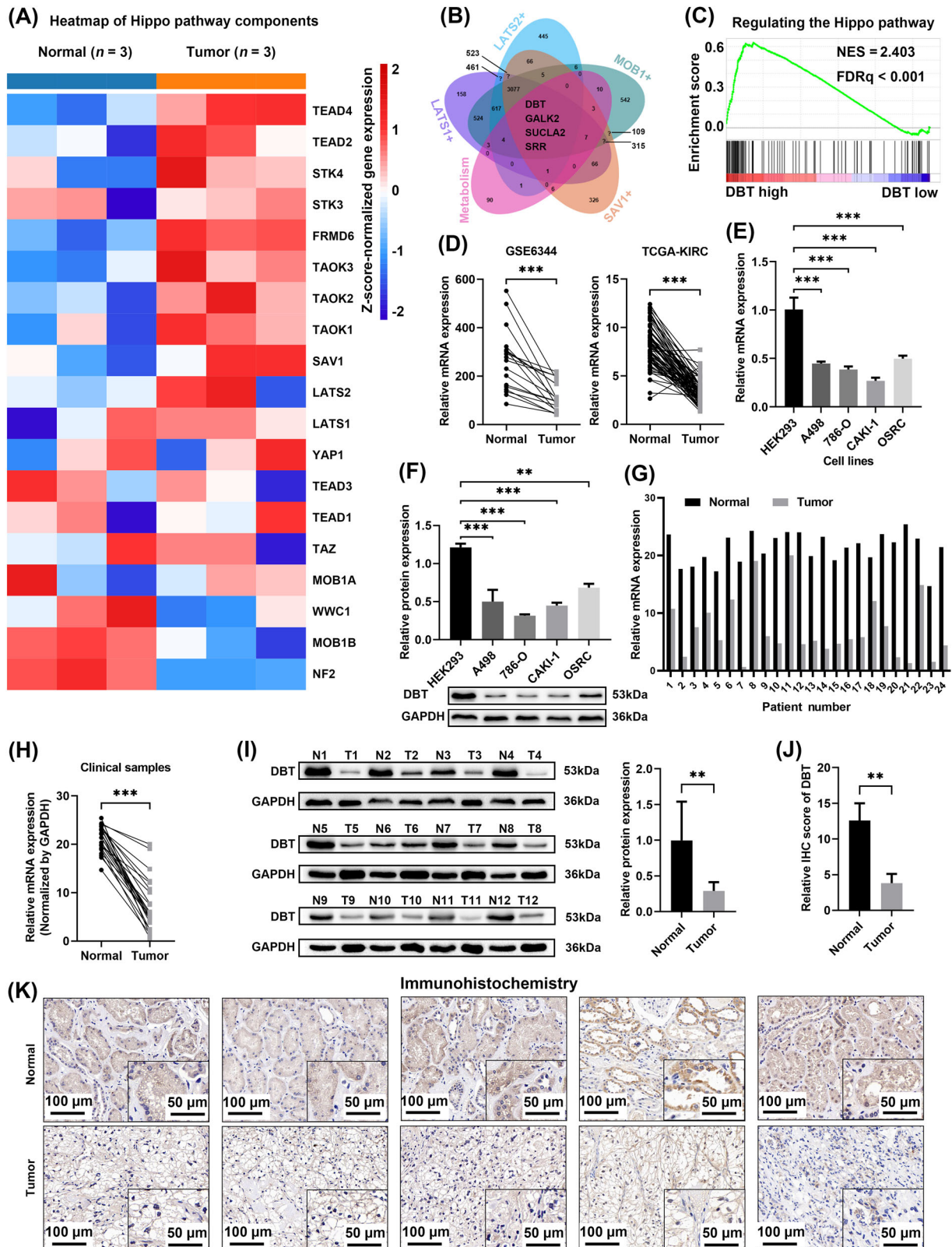
FIGURE 1 DBT was downregulated in ccRCC and indicated a poor prognosis. (A) Heatmap of 19 components of Hippo signaling in ccRCC tissues and paired adjacent normal tissues (*n* = 3). Each row represents a gene, each column represents a sample, and the color indicates the gene expression level normalized by row using "Z-score". (B) Venn diagram of the metabolism-related gene set and four Hippo-related gene sets from the Oncomine database (https://www.oncomine.org). "*LATS1*+" means that the correlation between this gene set and *LATS1* is greater than 0.35. (C) GSEA shows the association between *DBT* and the Hippo signaling pathway. FDR < 25% was considered statistically significant. (D) The mRNA levels of *DBT* in ccRCC tissues and paired adjacent normal tissues based on data from the

TABLE 1 Univariate and multivariate Cox analyses of overall survival of 534 patients with ccRCC.

Variable	Total (cases)	Univariate analysis			Multivariate analysis		
		HR	95% CI	P	HR	95% CI	P
Age (years)							
≤60	265	1.000			1.000		
>60	269	1.859	1.343-2.572	<0.001	1.754	1.264-2.433	0.001
Gender							
Female	185	1.000			1.000		
Male	349	0.916	0.662-1.267	0.596	1.169	0.840-1.627	0.353
T stage							
T1 & T2	347	1.000			1.000		
T3 & T4	187	1.875	1.596-2.204	<0.001	1.689	1.150-2.482	0.008
M stage							
M0	444	1.000			1.000		
M1	80	4.420	3.203-6.099	<0.001	2.926	1.833-4.672	<0.001
Mx	10						
N stage							
N0	236	1.000					
N1	16	2.906	1.499-5.633	0.002			
Nx	282						
Grade							
G1 & G2	247	1.000			1.000		
G3 & G4	280	1.676	1.394-2.017	0.005	1.463	1.124-1.904	0.005
Gx	7						
DBT expression							
Low	266	1.000			1.000		
High	268	0.546	0.384-0.756	<0.001	0.565	0.477-0.828	0.016

Mx, Nx, and Gx represent cases with missing data.

Multivariate models were adjusted for age, T stage, M stage, and Grade.

Abbreviations: *DBT*, dihydrolipoamide branched chain transacylase E2; HR, hazard ratio; CI, confidence interval.

3.3 | DBT suppressed the progression of ccRCC in vitro and in vivo

ccRCC cell lines with overexpression or knockdown of DBT were established to examine the biological function of DBT in ccRCC (Supplementary Figure S3A-B). The results of CCK8 cell viability assays presented that overexpression of DBT significantly inhibited cell proliferation in ccRCC cells (Figure 3A and Supplementary Figure S3C). On the contrary, DBT knockdown promoted cell proliferation (Supplementary Figure S3D-E). Colony formation assays denoted that DBT-overexpressed cells possessed decreased proliferation ability (Supplementary Figure S3F-G). Transwell assays indicated that the migration and invasion abilities of DBT-overexpressed cells were significantly reduced (Figure 3B and Supplementary Figure S3H). Concurrently, the depletion of DBT improved the migration and invasion abilities of A498 and CAKI-1 cells (Supplementary Figure S3I-J). Moreover, apoptotic cells were significantly increased in DBT-overexpressed

GEO database (GSE6344) and TCGA (KIRC) database (*t*-test for statistics). (E-F) mRNA and protein levels of *DBT* in ccRCC cell lines and a normal cell line (*n* = 3) (*t*-test for statistics). (G-H) The mRNA levels of *DBT* in ccRCC tissues and paired adjacent normal tissues from 24 patients (*t*-test for statistics). (I) The protein levels of DBT in ccRCC tissues and paired adjacent normal tissues (*n* = 12) (*t*-test for statistics). (J-K) Representative IHC staining for DBT in ccRCC tissues and adjacent normal tissues from 5 patients (*t*-test for statistics). Results represented at least three independent experiments (*$P < 0.05$, **$P < 0.01$, ***$P < 0.001$).

Abbreviations: *DBT*, dihydrolipoamide branched chain transacylase E2; ccRCC, clear cell renal cell carcinoma; *LATS1/2*, large tumor suppressor kinase 1/2; *MOB1*, MOB kinase activator 1; *SAV1*, salvador family WW domain containing protein 1; GSEA, gene set enrichment analysis; FDR, false discovery rate; NES, normalized enrichment score; GEO, gene expression omnibus; TCGA, the cancer genome atlas; KIRC, kidney renal clear cell carcinoma; *GAPDH*, glyceraldehyde-3-phosphate dehydrogenase; IHC, immunohistochemical.
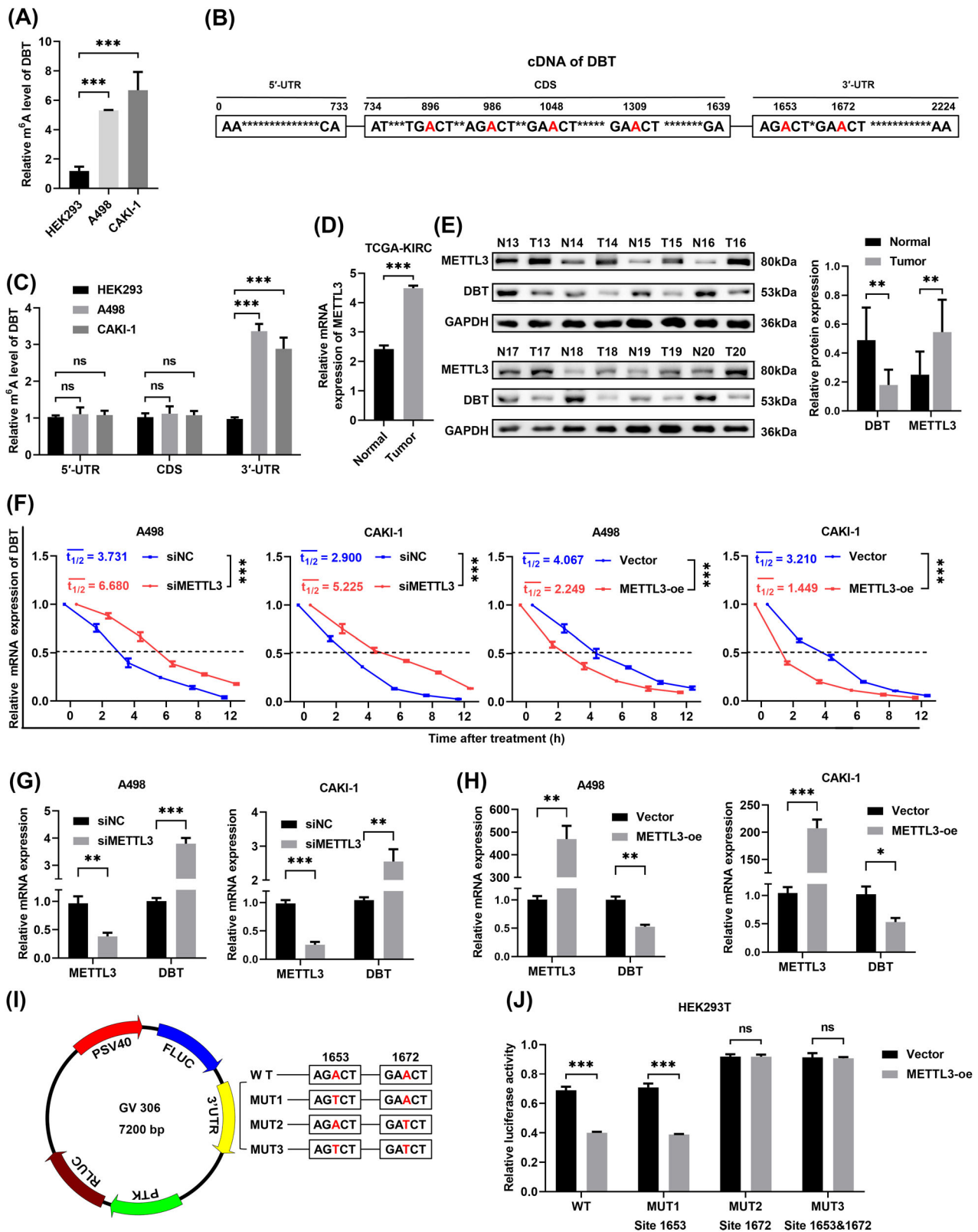
FIGURE 2 METTL3-mediated m^{6}A modification was involved in *DBT* downregulation. (A) The m^{6}A modification levels of *DBT* in ccRCC cell lines and a normal cell line ($n = 3$) (*t*-test for statistics). (B) The predicted m^{6}A modification sites of *DBT* using SRAMP. The "A" in red color is the potential modification site. (C) The m^{6}A modification levels of different regions in *DBT* between ccRCC cell lines and a normal cell line ($n = 3$) (*t*-test for statistics). (D) The mRNA levels of *METTL3* in ccRCC tissues and paired adjacent normal tissues using data from the TCGA database (*t*-test for statistics). (E) The protein levels of METTL3 and *DBT* in ccRCC tissues and paired adjacent normal tissues ($n = 8$) (*t*-test for statistics). (F) The decay rate of *DBT* mRNA after treatment with actinomycin D in A498 and CAKI-1 cells with METTL3

cells (Figure 3C) and were decreased in DBT-knockdown cells (Supplementary Figure S4A). Then CAKI-1 cells with DBT overexpression were injected into BALB/c nude mice, and tumor size was monitored every four days. The volume and weight of subcutaneous tumors from the mice mentioned above were significantly reduced compared with those from mice injected with CAKI-1 cells carrying the empty vector (Figure 3D and Supplementary Figure S4B-C). In addition, Ki67, the marker of cellular proliferation, was significantly decreased in the DBT-overexpressed group (Figure 3E-F). Live small animal fluorescent imaging assessed the metastatic ability of cancer cells on a tail vein metastasis model. The results suggested that overexpression of DBT significantly inhibited tumor metastasis (Figure 3G-H) and reduced the number of metastatic nodes in the liver (Supplementary Figure S4D). The above findings indicated that DBT had a tumor-suppressive role in ccRCC.

3.4 | DBT alleviated lipid accumulation in ccRCC

Remarkably, the most prominent biological feature of ccRCC is intracellular lipid droplet accumulation [39]. *DBT* was screened out in the present study since it is known to participate in metabolism. Therefore, GSEA was performed to confirm its role in cancer metabolism. The results revealed that DBT was involved in fatty acid metabolism (Figure 4A). This study then silenced and overexpressed DBT in A498 and CAKI-1 cells to test its potential effect on lipid metabolism in ccRCC. Oil red staining assays displayed that lipid accumulation was reduced in DBT-overexpressed cell lines (Figure 4B) while knockdown of DBT raised the lipid droplet levels (Figure 4C). Next, the TG concentration as another indicator of lipid accumulation was detected by using the TG assay kit. The results showed that cells with DBT overexpression exhibited a relatively lower TG content (Figure 4D). However, a higher TG content was observed in cells with DBT knockdown (Figure 4E), consistent with the Oil red staining assay. Additionally, the TG concentrations in subcutaneous tumors were measured. The result

suggested that overexpression of DBT reduced TG concentration in vivo (Figure 4F). The above findings concluded that DBT was a regulator of lipid accumulation of ccRCC.

3.5 | DBT activated Hippo signaling to repress the transcriptional activity of YAP

To examine the effect of DBT on the Hippo pathway in ccRCC, the RNA levels of the core components of the Hippo pathway were detected. According to the results, overexpression or knockdown of *DBT* presented no significant difference in Hippo signaling at the mRNA level (Supplementary Figure S5A-B). However, Western blotting assays demonstrated an increase of phosphorylated YAP in DBT-overexpressed cells (Figure 5A and Supplementary Figure S5C) while a decrease of phosphorylated YAP in DBT knockdown cells (Figure 5B and Supplementary Figure S5D). Moreover, overexpression of DBT reduced the nuclear YAP staining (Figure 5C and Supplementary Figure S5E). On the contrary, the knockdown of DBT elevated the YAP translocation into the nucleus (Supplementary Figure S5F). The Western blotting of nucleo-cytoplasmic separation demonstrated that overexpression of DBT inhibited YAP nuclear localization (Figure 5D and Supplementary Figure S6A) while knockdown of DBT inhibited YAP cytoplasmic localization (Figure 5E and Supplementary Figure S6B). These results indicated that DBT activated Hippo signaling, leading to the cytoplasmic localization of YAP.

It has been established that de novo lipid synthesis is the classical pathway for Hippo signaling to regulate lipid accumulation [16–18]. Thus, we compared the mRNA levels of genes that participated in lipid anabolism, lipid catabolism and fatty acid oxidation (FAO) in cells treated with the YAP inhibitor (verteporfin) or DMSO. The results supported current theories that fatty acid synthase (*FASN*), acetyl-CoA carboxylase (*ACC*) and peroxisome proliferator-activated receptor gamma (*PPARg*) were under the control of the Hippo pathway (Supplementary Figure S6C). Consistent with the conclusion that DBT was a regulator of lipid accumulation of ccRCC, we found that overexpression of DBT reduced the mRNA

knockdown or overexpression ($n = 3$) (t-test for statistics). (G) The mRNA expression level of *DBT* in ccRCC cells with METTL3 knockdown ($n = 3$) (t-test for statistics). (H) The mRNA expression level of *DBT* in ccRCC cells with METTL3 overexpression ($n = 3$) (t-test for statistics). (I) A schematic diagram shows wild-type *DBT* 3′-UTR and *DBT* 3′-UTR with mutations at the m^{6}A medication sites were cloned into a luciferase reporter. (J) Relative luciferase activity of the wild-type and mutant *DBT* 3′-UTR reporter vectors catalyzed by METTL3 ($n = 3$) (t-test for statistics). Results represented at least three independent experiments (*$P < 0.05$, **$P < 0.01$, ***$P < 0.001$).

Abbreviations: *DBT*, dihydrolipoamide branched chain transacylase E2; ccRCC, clear cell renal cell carcinoma; SRAMP, A sequence-based m^{6}A modification site predictor; *METTL3*, methyltransferase-like-3; TCGA, the cancer genome atlas; KIRC, kidney renal clear cell carcinoma; cDNA, complementary DNA; UTR, untranslated region; CDS, coding sequence; *GAPDH*, glyceraldehyde-3-phosphate dehydrogenase; WT, wild-type; MUT, mutation; FLUC, firefly luciferase; RLUC, renilla luciferase; ns, not significant.
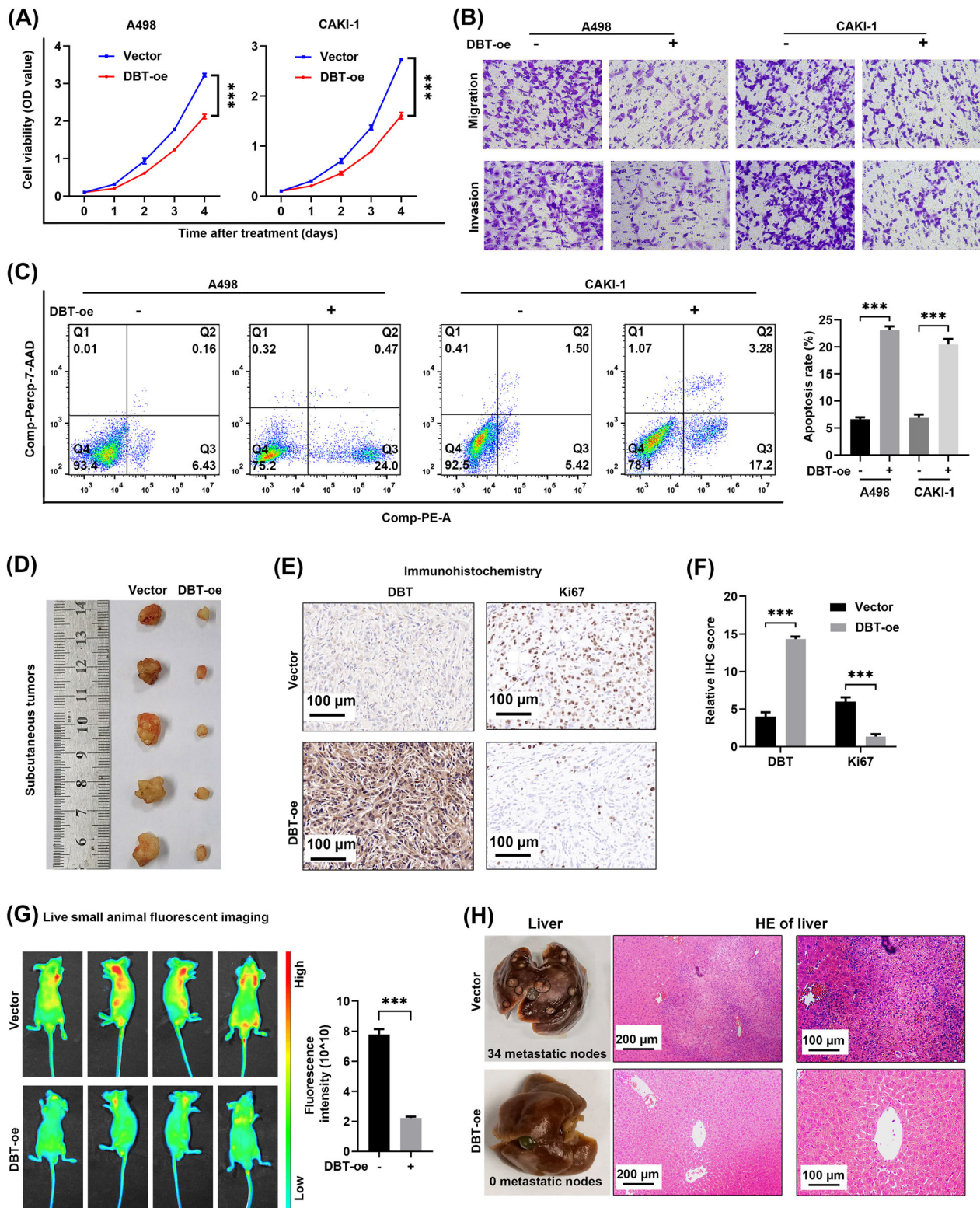
FIGURE 3 DBT suppressed the progression of ccRCC in vitro and in vivo. (A) Cell proliferation curves of CCK8 assays for the cell lines with DBT overexpression ($n = 4$) (t-test for statistics). (B) The results of Transwell assays for the DBT-overexpressed cells or the control cells ($n = 3$). (C) Flow cytometry assay showing the proportion of apoptotic cells in DBT-overexpressed ccRCC cells and the control cells ($n = 3$) (t-test for statistics). Comp-PE-A means Annexin V was compensated by negative control and single positive control. Comp-Percp-7-AAD means 7-AAD was compensated by negative control and single positive control. (D) CAKI-1 cells with stable DBT overexpression were injected into nude mice. Tumors were extracted after mice were euthanized. (E) IHC staining for DBT and Ki67 in the isolated subcutaneous tumors. (F) IHC score of DBT and Ki67 in subcutaneous tumors from the DBT-overexpressed group and the control group ($n = 3$) (t-test for statistics). (G) Live small animal fluorescent images of the metastasis model in the DBT-overexpressed group and control group ($n = 3$) (t-test

(Supplementary Figure S7A) and protein levels of *FASN*, *ACC* and *PPARg* (Supplementary Figure S7B). Conversely, DBT knockdown elevated the mRNA (Supplementary Figure S7C) and protein levels of lipid anabolism genes (Supplementary Figure S7D-E). Next, ccRCC cells with DBT knockdown were treated with verteporfin to authenticate that Hippo signaling was critical in DBT-mediated lipid accumulation and tumor suppression. Here, connective tissue growth factor (CTGF) is regarded as a known marker of YAP inhibition [40]. Firstly, we confirmed that the protein expression of DBT was not influenced by verteporfin (Supplementary Figure S8A). Then, Western blotting showed that YAP inhibition significantly alleviated the upregulation of CTGF, FASN, ACC and PPARg in cells with DBT knockdown (Figure 5F and Supplementary Figure S8B-C). Furthermore, it demonstrated that YAP inhibition significantly reduced the lipid accumulation induced by the knockdown of DBT (Supplementary Figure S8D-E). Next, Transwell assays showed that when induced by verteporfin, YAP inhibition significantly alleviated the promotion of invasion and migration abilities of cells with DBT knockdown (Figure 5G and Supplementary Figure S9A-B). Similarly, YAP inhibition offset the promotion of proliferation caused by DBT knockdown (Figure 5H and Supplementary Figure S9C). Moreover, YAP inhibition significantly rescued the apoptosis-resistant phenotype induced by the knockdown of DBT (Figure 5I and Supplementary Figure S9D-E). These results confirmed that DBT activated the Hippo pathway and then repressed lipid accumulation and tumor progression in ccRCC.

3.6 | DBT regulated Hippo signaling by interacting with ANXA2

Most proteins, including DBT, function in the context of complexes [22, 24], and the Hippo pathway network is a classic example as it is under the control of various interactions between proteins [26]. Thus, immunoprecipitation (IP) and MS experiments were conducted to determine how DBT regulated the Hippo pathway. Briefly, Flag-tagged DBT or vector was overexpressed in HEK293T cells (Figure 6A and Supplementary Figure S10A), and IP followed by MS analyses was performed. The proteins pulled down through Flag-DBT but not by vector are shown in Supplementary Table S5. A previous study [26] reported numerous new protein interactions for YAP and proposed that these interactions provided insight into

the detailed mechanisms underlying the Hippo pathway. We attempted to identify the link between DBT and YAP by combining the proteins that interacted with YAP in the previous study [22, 26] with the proteins pulled down through Flag-DBT (Figure 6B). Among the 12 candidates, ANXA2 is one of the annexin family members with multiple roles in cell proliferation, membrane physiology, and tumor progression [41]. To confirm the function of ANXA2 in ccRCC, shRNA targeting *ANXA2* was designed (Supplementary Figure S10B). The depletion of ANXA2 enhanced the abilities of proliferation (Figure 6C and Supplementary Figure S10C-E), invasion and migration (Supplementary Figure S10F-G) in A498 and CAKI-1 cells. Moreover, the proportion of apoptotic cells was significantly decreased by knockdown of ANXA2 in ccRCC cells (Figure 6D and Supplementary Figure S10H-I). More importantly, ANXA2 was reported to interact with Hippo pathway proteins [26, 42], and it shepherded YAP to the membrane where YAP was inhibited by phosphorylation [42]. We found that knockdown of ANXA2 contributed to a decreased phosphorylation of YAP and improved transcriptional activity of lipogenic genes, such as FASN and ACC (Supplementary Figure S10J-K), which led to an increase in lipid accumulation (Supplementary Figure S10L). Next, we hypothesized that ANXA2 mediated the tumor suppressive effect of DBT in ccRCC. Consistent with previous results, DBT overexpression led to the activation of Hippo signaling and increased phosphorylation of YAP (Supplementary Figure S11A), resulting in decreased expression of downstream lipogenic genes. Then, shRNA target *ANXA2* was transfected into DBT-overexpressed cells. Western blotting demonstrated that the depletion of ANXA2 rescued the changes induced by DBT overexpression (Supplementary Figure S11A). Additionally, the Oil red staining and TG detection assays exhibited that the decreased lipid storage due to overexpression of DBT in ccRCC was partially restored by the depletion of ANXA2 (Supplementary Figure S11B and S12A). Moreover, ANXA2 silencing significantly alleviated the inhibition of proliferation caused by DBT overexpression (Supplementary Figure S12B-E). Similarly, knockdown of ANXA2 reestablished invasion and migration abilities in DBT-overexpressed cells (Supplementary Figure S12F). Moreover, it showed that cell apoptosis induced by overexpression of DBT was significantly suppressed by ANXA2 knockdown (Supplementary Figure S13A). These results confirmed that DBT suppressed cancer progression and lipid accumulation through the ANXA2-regulated Hippo pathway.

---

for statistics). (H) H&E staining of the liver tissues from the metastasis model in DBT-overexpressed and control groups. Results represented at least three independent experiments (*$P < 0.05$, **$P < 0.01$, ***$P < 0.001$).

Abbreviations: *DBT*, dihydrolipoamide branched chain transacylase E2; CCK8, cell counting kit 8; OD, optical density; IHC, immunohistochemical; H&E, hematoxylin-eosin; PE, phycoerythrin; 7-AAD, 7-amino-actinomycin D.
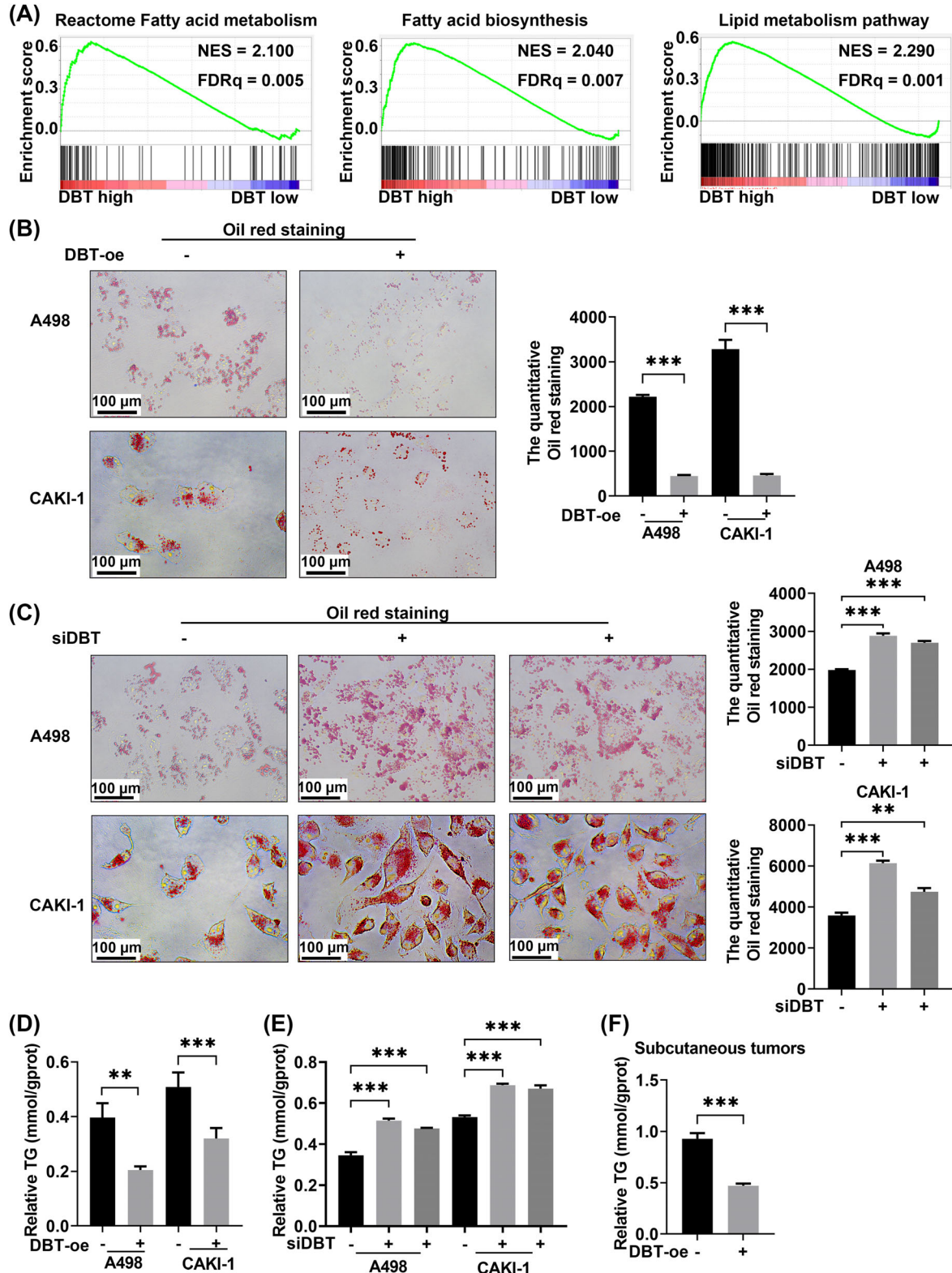
FIGURE 4 DBT alleviated lipid accumulation in ccRCC. (A) GSEA showed the associations between the lipid metabolism in ccRCC and the *DBT* mRNA levels. FDR < 25% was considered statistically significant. (B) Photomicrographs of Oil red staining of the DBT-overexpressed cell lines compared with the negative control (*n* = 3) (*t*-test for statistics). (C) Photomicrographs of Oil red staining in cells with DBT knockdown (*n* = 3) (*t*-test for statistics). (D) Relative TG (mmol/gprot) levels in cells with DBT overexpression were assessed by a TG assay kit (*n* = 3) (*t*-test for statistics). (E) Relative TG (mmol/gprot) levels in cells with DBT knockdown were assessed by a TG assay kit (*n* = 3) (*t*-test for statistics). (F) Relative TG (mmol/gprot) levels in subcutaneous tumors in the DBT-overexpressed group and the control group by a TG assay kit (*n* = 5) (*t*-test for statistics). Results represented at least three independent experiments (*P < 0.05, **P < 0.01, ***P < 0.001). Abbreviations: *DBT*, dihydrolipoamide branched chain transacylase E2; GSEA, gene set enrichment analysis; FDR, false discovery rate; NES, normalized enrichment score; TG, triglyceride.
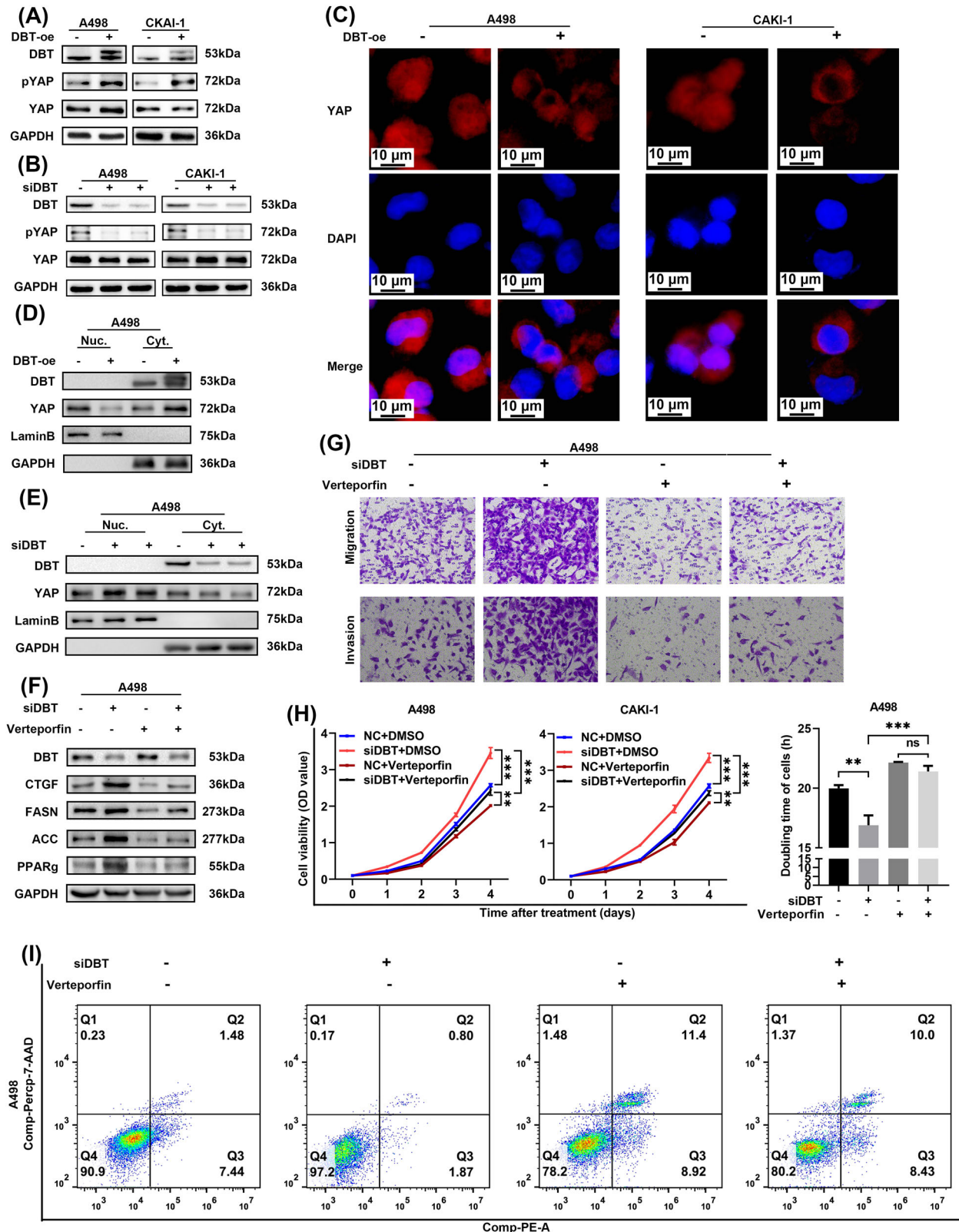
FIGURE 5 DBT activated Hippo signaling to repress the transcriptional activity of YAP. (A) Western blotting shows the levels of phosphorylated YAP and total YAP in DBT-overexpressed cells and control cells. (B) Western blotting shows the levels of phosphorylated YAP and total YAP in DBT-knockdown cells and control cells. (C) Immunofluorescence assays display subcellular localization of YAP after DBT overexpression. (D) Western blotting shows subcellular localization of YAP after DBT overexpression. (E) Western blotting shows subcellular localization of YAP after DBT knockdown. (F) Western blotting shows protein levels of DBT and lipogenic genes, such as FASN and ACC, in the indicated cell lines. Cells with DBT knockdown were treated with 10 μmol/L verteporfin (an inhibitor of YAP-TEAD) or DMSO. (G) Transwell assays were conducted for the indicated ccRCC cell lines. Cells with DBT knockdown were treated with 10 μmol/L verteporfin or

A series of co-IP assays were performed to clarify how DBT/ANXA2 regulated the Hippo pathway. In HEK293T cells, it was discovered that endogenous DBT was efficiently immunoprecipitating ANXA2 and endogenous ANXA2 was also efficiently immunoprecipitating DBT (Figure 6E). To further confirm this interaction, Flag-DBT and Myc-ANXA2 were overexpressed in HEK293T cells. It was revealed that Flag-DBT and Myc-ANXA2 could be immunoprecipitated with each other in HEK293T cells (Figure 6F-G). Next, co-IP assays were repeated in A498 and CAKI-1 cells (Figure 6H), results of which indicated that both DBT and YAP could be immunoprecipitated by Myc-ANXA2. To detect the binding domain for DBT interacting with ANXA2, we identified domains with the online tool (Intropro) based on the amino acid sequence of *DBT*. Then five Flag-tagged DBT parts (Figure 6I) were cloned. HEK293T cells were transfected with these truncated plasmids. Among all the Flag-tagged DBT parts, only Flag-P2 interacted with ANXA2 (Figure 6J), suggesting that the lipoyl-binding domain between amino acids 64 and 139 was mandatory for the interaction with ANXA2. These results showed that DBT physically interacted with ANXA2 to activate the Hippo pathway. We next sought to define how the interaction of DBT and ANXA2 could affect the phosphorylation of YAP. We observed that ANXA2 immunoprecipitated more YAP proteins in DBT-overexpressed cells (Figure 6K). Also, the lane of Input denoted that overexpression of DBT led to an increase in YAP phosphorylation. On the contrary, knockdown of DBT commanded less interaction between ANXA2 and YAP and decreased YAP phosphorylation (Figure 6L). It has been reported that the biological functions of ANXA2 were regulated by a variety of post-translational modifications [43–45], such as ubiquitination and phosphorylation. To further investigate whether DBT affected the stability of ANXA2, ccRCC cells were treated with cycloheximide, an inhibitor of protein biosynthesis. The results of the cycloheximide chase assay showed that the protein stability of ANXA2 was not influenced by DBT overexpression (Supplementary Figure S13B). Then, we explored whether DBT regulated the biological activity of ANXA2 by affecting its phosphorylation. By measuring the abundances of total

ANXA2 and phosphorylated ANXA2 in ccRCC cells, it was found that DBT overexpression led to an increase of phosphorylated ANXA2 in A498 and CAKI-1 cells (Supplementary Figure S13C). Since the phosphorylation of ANXA2 is required for the membrane localization of the ANXA2 [43], we suspected that DBT might affect the cellular localization of ANXA2. Thus, membrane-cytoplasmic protein separation assays were conducted. The results showed that DBT overexpression induced the translocalization of ANXA2 to the cell membrane (Supplementary Figure S13D), where ANXA2 promotes the phosphorylation of YAP. These data suggested that DBT directly bound to ANXA2 and promotes its normal cellular function of repressing YAP activity.

3.7 | The DBT-ANXA2-YAP axis suppressed tumor progression and lipid accumulation in vivo

Next, the function of the DBT-ANXA2-YAP axis was investigated in vivo via subcutaneous tumor models and metastatic tumor models. The results of subcutaneous tumor models indicated that DBT overexpression yielded effective inhibition of tumor growth as compared to the vector group, while the knockdown of ANXA2 could reverse the growth inhibition caused by DBT overexpression (Figure 7A), consistent with in vitro experiments. The same conclusions were also drawn from results of tumor weights and tumor volumes (Figure 7B-C). Moreover, the IHC assays of isolated tumors from subcutaneous tumor models showed that the declined expression of Ki67, FASN, ACC and PPARg in the DBT-overexpressed group was partially restored via the depletion of ANXA2 (Figure 7D-E). Live small animal fluorescent imaging assays showed that the depletion of ANXA2 reversed the metastasis inhibition effect caused by DBT overexpression (Figure 7F-G). Also, knockdown of ANXA2 put on the number of metastatic nodes in mouse livers of the DBT-overexpressed group (Figure 7H). Furthermore, the depletion of ANXA2 could block the decrease of TG content in subcutaneous tumors induced by DBT overexpression (Figure 7I). These

DMSO. (H) Cell proliferation curves of CCK8 assays for indicated cell lines ($n = 4$) (*t*-test for statistics). The doubling time for indicated cell lines ($n = 4$) (*t*-test for statistics). Cells with DBT knockdown were treated with 10 μmol/L verteporfin or DMSO. (I) Flow cytometry assay showing the proportion of apoptotic cells for the indicated cell lines ($n = 3$). Cells with DBT knockdown were treated with 10 μmol/L verteporfin or DMSO. Comp-PE-A means Annexin V was compensated by negative control and single positive control. Comp-Percp-7-AAD means 7-AAD was compensated by negative control and single positive control. Results represented at least three independent experiments (*$P < 0.05$, **$P < 0.01$, ***$P < 0.001$).

Abbreviations: *DBT*, dihydrolipoamide branched chain transacylase E2; *YAP*, yes1-associated transcriptional regulator; *GAPDH*, glyceraldehyde-3-phosphate dehydrogenase; DAPI, 4',6-diamidino-2-phenylindole; *FASN*, fatty acid synthase; *ACC*, acetyl-CoA carboxylase; *PPARg*, peroxisome proliferator activated receptor gamma; *TEAD*, TEA domain transcription factor; DMSO, dimethyl sulfoxide; CCK8, cell counting kit 8; OD, optical density; NC, negative control; PE, phycoerythrin; 7-AAD, 7-amino-actinomycin D; ns, not significant.
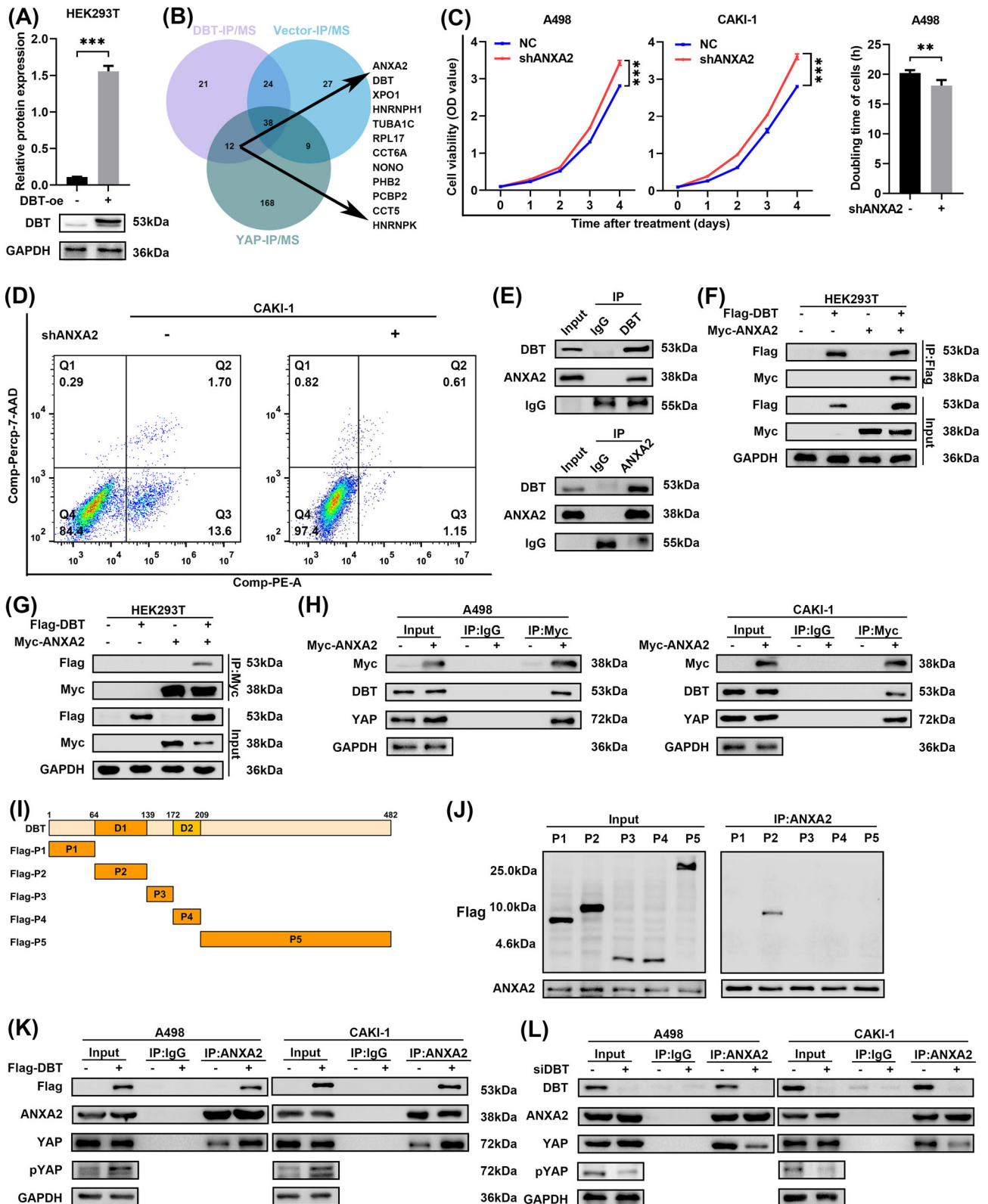
FIGURE 6 DBT regulated Hippo signaling by interacting with ANXA2. (A) DBT-overexpressed cell lines were constructed in HEK293T by Flag-DBT lentivirus. The overexpression of DBT was verified at the protein level using Western blotting ($n = 3$) (t-test for statistics). (B) Venn diagram of proteins interacted with YAP in Simon Hauri's study, proteins pulled down through Flag-DBT and proteins pulled down through Vector. (C) Cell proliferation curves of CCK8 assays for the cell lines with ANXA2 knockdown. The doubling time of cell lines with ANXA2 knockdown ($n = 4$) (t-test for statistics). (D) Flow cytometry assay showing the proportion of apoptotic cells with ANXA2 knockdown and the control cells ($n = 3$). Comp-PE-A means Annexin V was compensated by negative control and single positive control.

observations suggested that the DBT-ANXA2-YAP axis suppressed tumor progression and inhibited lipid accumulation in ccRCC.

4 | DISCUSSION

Here, this study reported a link between DBT and lipid accumulation in ccRCC (Figure 8). The m^6A modification-mediated DBT bound to ANXA2, resulting in activating the Hippo pathway and repressing the transcription of downstream lipogenic genes. Functional studies confirmed that the DBT/ANXA2/YAP axis was a key regulator of lipid biosynthesis and tumor progression in ccRCC.

RNA methylation, which influences gene expression and protein translation, is gradually emerging as a new therapeutic target in cancers [46]. N6-methyladenosine is the most important RNA modification that inhibits the expression of tumor suppressor genes by affecting pre-mRNA splicing and RNA stability [36, 37]. METTL3, functions as the "writer" of m^6A, is a core component of the N6-methyladenosine methyltransferase complex [37]. In various cancers, METTL3 sustained mRNA stabilization of targeted genes in an m^6A-dependent manner [37, 47]. Thus, METTL3 has been one of the most enticing targets for m^6A regulators of cancer treatment. Earlier studies verified that METTL3-depleted cancer cells were more sensitive to traditional anticancer therapy and that METTL3-mediated m^6A modification promoted T-cell activation in cancer immunotherapy [48]. Additionally, biotech companies have been developing selective inhibitors targeting METTL3 [48]. Interestingly, an increasing number of researchers demonstrated that m^6A modification played an important role in tumor metastasis, metabolism reprogramming and anticancer therapy of ccRCC [46, 49, 50], but the detailed underlying mechanism has not been well understood. Here, the present study illustrated that METTL3-mediated m^6A modification in the 3′-UTR contributed to the downregulated expression of *DBT* that subsequently functioned as a suppressor of tumor progression and lipid accumulation in ccRCC. This observation established a new mechanism for how METTL3-mediated m^6A modification functions in ccRCC and laid the groundwork for the development of drugs targeting the m^6A modification site of *DBT*.

Lipid metabolism reprogramming is a well-documented phenomenon with great significance in ccRCC. For example, proliferating cancer cells relied on fatty acids to provide ingredients for membrane and organelle formation [51], and lipid accumulation prevented cancer cells from reactive oxygen species-induced cytotoxicity [52]. Therefore, a growing body of literature is devoted to elucidating the causes of lipid accumulation in ccRCC. They proposed that inhibition of FAO and obstruction of decomposition were the top reasons for fatty acid accumulation and the development of ccRCC [53, 54]. Previous studies suggested that ccRCC cells consumed lipid storage via uncoupling protein 1 (*UCP1*)-mediated lipid browning [31, 53]. Although inhibition of lipid consumption and lipid browning were simultaneously observed in ccRCC, enhanced fatty acid synthesis mediated by the upregulated expression of rate-limiting enzymes in the de novo synthesis pathway also contributed to lipid accumulation in ccRCC [55]. The present study described DBT as a tumor suppressor which prevented lipid accumulation of ccRCC by transcriptional repression of the de novo synthesis pathway. Consistent with the notion that lipid metabolism itself is an attractive therapeutic target via inhibition of lipogenic enzymes [56], the present study provides a new explanation for lipid accumulation in ccRCC and a theoretical foundation for developing drugs that target lipid de novo synthesis.

The Hippo signaling pathway has been associated with controlling organ size and the development of cancer [11]. YAP is the chief downstream effector of the Hippo pathway that regulates the expression of many target genes [14]. Recent studies showed that YAP activation promoted ccRCC by inducing the epithelial-mesenchymal transition and regulating cell cycle distribution [57, 58]. Unlike other tumor suppressors, loss-of-function mutations in Hippo pathway components were less common in human cancers [35], indicating that an alternative mechanism for

Comp-Percp-7-AAD means 7-AAD was compensated by negative control and single positive control. (E) The endogenous DBT-ANXA2 interaction was determined by co-IP assays in HEK293T cells. (F-G) The exogenous DBT-ANXA2 interaction was determined by co-IP assays in HEK293T cells overexpressed Flag-DBT and/or Myc-ANXA2. (H) The DBT/YAP-ANXA2 interaction was determined by co-IP assays in A498 and CAKI-1 cells with Myc-ANXA2 overexpression. (I) The diagrams show wild-type DBT (full length, 1-482) and its five truncations. (J) HEK293T cells were transfected with the indicated truncated plasmids, followed by co-IP assays and Western blotting to examine the interaction between ANXA2 and DBT truncations. (K) The DBT/YAP-ANXA2 interaction was determined by co-IP assays in DBT-overexpressed cell lines. (L) The DBT/YAP-ANXA2 interaction was determined by co-IP assays in cell lines with DBT knockdown. Results represented at least three independent experiments (*$P < 0.05$, **$P < 0.01$, ***$P < 0.001$).

Abbreviations: *DBT*, dihydrolipoamide branched chain transacylase E2; *GAPDH*, glyceraldehyde-3-phosphate dehydrogenase; *ANXA2*, annexin A2; *YAP*, yes1-associated transcriptional regulator; CCK8, cell counting kit 8; OD, optical density; co-IP, co-immunoprecipitation; MS, mass spectrometry; PE, phycoerythrin; 7-AAD, 7-amino-actinomycin D.
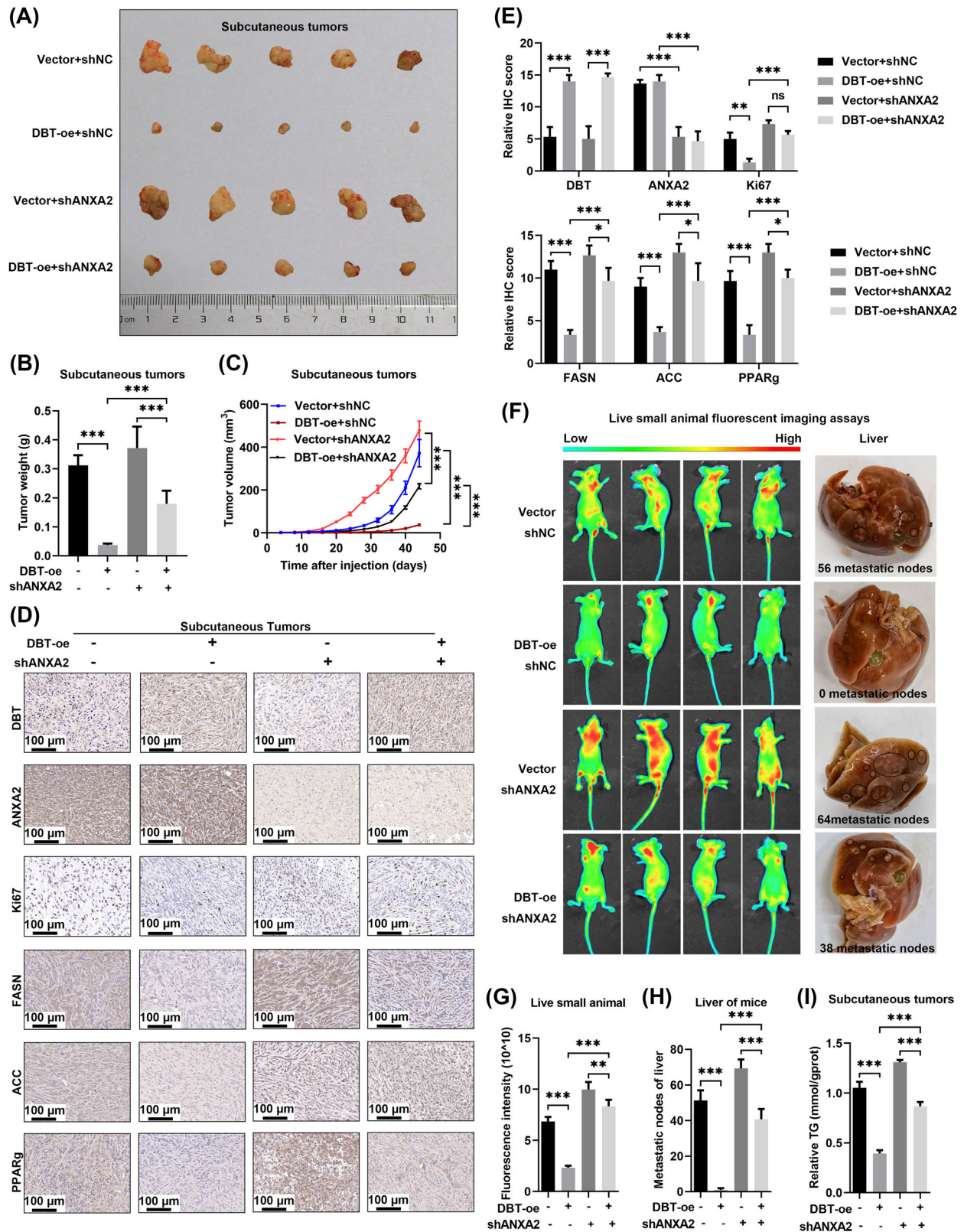
FIGURE 7 The DBT-ANXA2-YAP axis suppressed tumor progression and lipid accumulation in vivo. (A) Representative images of isolated subcutaneous tumors from nude mice. (B) Tumors were extracted and weighed after mice were euthanized ($n = 5$) (t-test for statistics). (C) Tumor size was measured every 4 days and the last measurement was performed on day 44 ($n = 5$) (t-test for statistics). (D-E) IHC staining for DBT, ANXA2, FASN, ACC and PPARg and Ki67 in the subcutaneous tumors ($n = 3$) (t-test for statistics). (F-G) Live small animal fluorescent images of the Vector + NC, DBT-oe + NC, Vector + shANXA2, and DBT-oe + shANXA2 groups in the metastasis model ($n = 3$) (t-test for statistics). (H) The number of metastatic nodes was counted on all sides of the liver ($n = 3$) (t-test for statistics). (I) Relative TG (mmol/gprot) levels in subcutaneous tumors cells in the Vector + NC, DBT-oe + NC, Vector + shANXA2, DBT-oe + shANXA2 groups were

assessed by a TG assay kit ($n = 3$) (*t*-test for statistics). Results represented at least three independent experiments (*$P < 0.05$, **$P < 0.01$, ***$P < 0.001$).

Abbreviations: *DBT*, dihydrolipoamide branched chain transacylase E2; *ANXA2*, annexin A2; *IHC*, immunohistochemical; *FASN*, fatty acid synthase; *ACC*, acetyl-CoA carboxylase; *PPARg*, peroxisome proliferator activated receptor gamma; *TG*, triglyceride; *NC*, negative control; *ns*, not significant.

regulating the Hippo pathway exists in the progression of ccRCC, such as targeting the expression and/or phosphorylation of YAP. Here, we identified a moonlighting function of DBT for regulating the Hippo pathway. The interaction of DBT and ANXA2 provided a basic explanation for how DBT participated in the ANXA2-mediated phosphorylation of YAP. A body of evidence shows that the biological function of ANXA2 was regulated by a variety of post-translational modifications [43–45]. In the present study, DBT simultaneously upregulated the phosphorylation and membrane localization of ANXA2. It is well known that the phosphorylation of ANXA2 is required for its translocation to the membrane [43]. Thus, we speculated that DBT might regulate the subcellular localization of ANXA2 by affecting its phosphorylation, thereby facilitating ANXA2-mediated YAP inhibition. Nowadays, the options for pharmacological treatment of RCC include

immune checkpoint inhibitors (ICIs) and inhibition of the vascular endothelial growth factor (VEGF)/mammalian target of rapamycin (mTOR) pathway [2]. Although ICIs improve outcomes for patients with metastatic RCC, patients still develop resistance to such therapies [2]. Thus, the development of novel therapeutic strategies is essential. Numerous drugs targeting YAP have been applied in clinical practice, which are reported to have better outcomes in patients with various cancers compared to traditional kinase inhibitors such as dasatinib [59]. Therefore, based on the findings in the present study, it is highly practicable that ICIs-based and Hippo-targeted combination therapy may achieve better outcomes in ccRCC patients.

There were several limitations in our study. Although DBT was validated to inhibit lipid accumulation of ccRCC through the Hippo signaling, the detailed mechanism of how DBT downregulation-mediated lipid accumula-
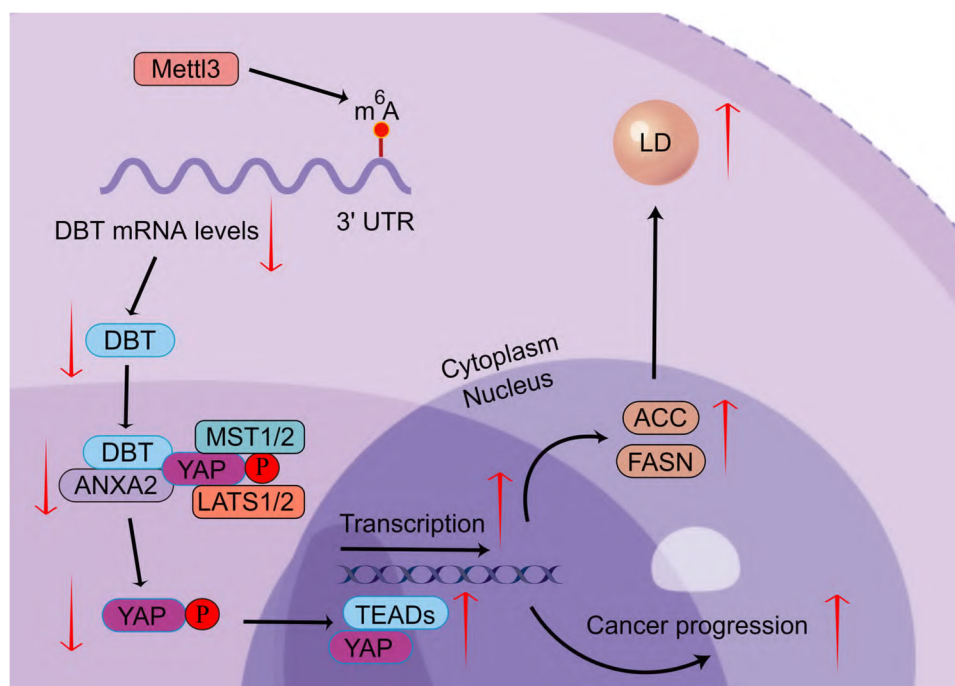

FIGURE 8 The mechanism scheme of DBT in ccRCC. METTL3-mediated m⁶A methylation reduces the expression of *DBT* in ccRCC; DBT interacts with ANXA2 to facilitate its shepherding YAP to the membrane where YAP is phosphorylated, thereby activating the Hippo pathway. Then the DBT/ANXA2/YAP axis-regulated Hippo pathway promotes the progression and lipid accumulation in ccRCC. The mechanism scheme was drawn by using Figdraw (www.figdraw.com).

Abbreviations: *METTL3*, methyltransferase-like-3; *UTR*, untranslated region; *DBT*, dihydrolipoamide branched chain transacylase E2; *ANXA2*, annexin A2; *YAP*, yes1-associated transcriptional regulator; *LATS1/2*, large tumor suppressor kinase 1/2; *MST1/2*, macrophage stimulating 1/2; *TEAD*, TEA domain transcription factor; *FASN*, fatty acid synthase; *ACC*, acetyl-CoA carboxylase; *LD*, lipid droplet.

tion promoted ccRCC progression should be more sufficiently explained. Besides, whether there existed m^{6}A-independent pathways that contributed to DBT downregulation in ccRCC could be further explored.

5 | CONCLUSIONS

The present study indicated a role of DBT in regulating the Hippo pathway by interacting with ANXA2 which shepherds YAP to be inhibited by phosphorylation. Aberrant downregulation of *DBT*, induced by METTL3-mediated m^{6}A modification, promotes the progression and lipid accumulation of ccRCC through the increased nuclear localization of YAP. Thus, the present study revealed an essential regulatory mechanism for regulating YAP activity and lipid metabolism in ccRCC, and provided an opportunity for developing therapeutic strategies for ccRCC treatment by targeting either YAP or *DBT* m^{6}A modification.

AUTHOR CONTRIBUTIONS
XZ and ZX designed and directed data processing procedures. DM, JS, QW, QL, DT and CZ analyzed the data. DM wrote the manuscript. All authors read and approved the final manuscript.

ACKNOWLEDGEMENTS
The authors have nothing to report.

CONFLICT OF INTEREST STATEMENT
The authors declare no potential conflicts of interest. All participants agreed to publish this article.

DECLARATIONS
ETHICS APPROVAL AND CONSENT TO PARTICIPATE
The tissue samples were obtained with written informed consent from each patient, and this study was approved by the Institutional Review Board of Huazhong University of Science and Technology (IEC-072). All animal studies were approved by the Institutional Animal Use and Care Committee of Tongji Medical College (S1892).

DATA AVAILABILITY STATEMENT
The datasets generated and analyzed during the current study are available in the TCGA repository (https://portal.gdc.cancer.gov) and GEO database (GSE6344, https://www.ncbi.nlm.nih.gov/gds). Other data generated in this study are available upon request from the corresponding author.

CONSENT FOR PUBLICATION
Written informed consent was obtained from patients for the publication of their data.

ORCID
Xiaoping Zhang https://orcid.org/0000-0003-0218-3288

REFERENCES
1. Hsieh JJ, Purdue MP, Signoretti S, Swanton C, Albiges L, Schmidinger M, et al. Renal cell carcinoma Renal cell carcinoma. Nat Rev Dis Primers. 2017;3:17009.
2. Choueiri TK, Motzer RJ. Systemic Therapy for Metastatic Renal-Cell Carcinoma. N Engl J Med. 2017;376(4):354-66.
3. Escudier B, Porta C, Schmidinger M, Rioux-Leclercq N, Bex A, Khoo V, et al. Renal cell carcinoma: ESMO Clinical Practice Guidelines for diagnosis, treatment and follow-up. Ann Oncol. 2016;27(suppl 5):v58-v68.
4. Barata PC, Rini BI. Treatment of renal cell carcinoma: Current status and future directions. CA Cancer J Clin. 2017;67(6):507-24.
5. Pham DV, Park PH. Adiponectin triggers breast cancer cell death via fatty acid metabolic reprogramming. J Exp Clin Cancer Res. 2022;41(1):9.
6. Xu H, Chen Y, Gu M, Liu C, Chen Q, Zhan M, et al. Fatty Acid Metabolism Reprogramming in Advanced Prostate Cancer. Metabolites. 2021;11(11):765.
7. Wettersten HI, Aboud OA, Lara PN, Jr., Weiss RH. Metabolic reprogramming in clear cell renal cell carcinoma. Nat Rev Nephrol. 2017;13(7):410-9.
8. Hakimi AA, Reznik E, Lee CH, Creighton CJ, Brannon AR, Luna A, et al. An Integrated Metabolic Atlas of Clear Cell Renal Cell Carcinoma. Cancer Cell. 2016;29(1):104-16.
9. Tan SK, Welford SM. Lipid in Renal Carcinoma: Queen Bee to Target? Trends Cancer. 2020;6(6):448-50.
10. Linehan WM, Schmidt LS, Crooks DR, Wei D, Srinivasan R, Lang M, et al. The Metabolic Basis of Kidney Cancer. Cancer Discov. 2019;9(8):1006-21.
11. Pan D. The hippo signaling pathway in development and cancer. Dev Cell. 2010;19(4):491-505.
12. Halder G, Johnson RL. Hippo signaling: growth control and beyond. Development. 2011;138(1):9-22.
13. Zhao B, Li L, Lei Q, Guan KL. The Hippo-YAP pathway in organ size control and tumorigenesis: an updated version. Genes Dev. 2010;24(9):862-74.
14. Meng Z, Moroishi T, Guan KL. Mechanisms of Hippo pathway regulation. Genes Dev. 2016;30(1):1-17.
15. Dey A, Varelas X, Guan KL. Targeting the Hippo pathway in cancer, fibrosis, wound healing and regenerative medicine. Nat Rev Drug Discov. 2020;19(7):480-94.
16. Koo JH, Guan KL. Interplay between YAP/TAZ and Metabolism. Cell Metab. 2018;28(2):196-206.
17. Jeong SH, Kim HB, Kim MC, Lee JM, Lee JH, Kim JH, et al. Hippo-mediated suppression of IRS2/AKT signaling prevents hepatic steatosis and liver cancer. J Clin Invest. 2018;128(3):1010-25.
18. Ibar C, Irvine KD. Integration of Hippo-YAP Signaling with Metabolism. Dev Cell. 2020;54(2):256-67.

19. Piccolo S, Dupont S, Cordenonsi M. The biology of YAP/TAZ: hippo signaling and beyond. Physiol Rev. 2014;94(4): 1287-312.

20. Yang WH, Ding CC, Sun T, Rupprecht G, Lin CC, Hsu D, et al. The Hippo Pathway Effector TAZ Regulates Ferroptosis in Renal Cell Carcinoma. Cell Rep. 2019;28(10):2501-8 e4.

21. Yin L, Li W, Wang G, Shi H, Wang K, Yang H, et al. NR1B2 suppress kidney renal clear cell carcinoma (KIRC) progression by regulation of LATS 1/2-YAP signaling. J Exp Clin Cancer Res. 2019;38(1):343.

22. Lackey DE, Lynch CJ, Olson KC, Mostaedi R, Ali M, Smith WH, et al. Regulation of adipose branched-chain amino acid catabolism enzyme expression and cross-adipose amino acid flux in human obesity. Am J Physiol Endocrinol Metab. 2013;304(11):E1175-87.

23. Friedrich T, Lambert AM, Masino MA, Downes GB. Mutation of zebrafish dihydrolipoamide branched-chain transacylase E2 results in motor dysfunction and models maple syrup urine disease. Dis Model Mech. 2012;5(2):248-58.

24. Zeng H, Wang S, Zhou T, Zhao F, Li X, Wu Q, et al. ComplexContact: a web server for inter-protein contact prediction using deep learning. Nucleic Acids Res. 2018;46(W1): W432-W7.

25. Ahn SH, Yang HY, Tran GB, Kwon J, Son KY, Kim S, et al. Interaction of peroxiredoxin V with dihydrolipoamide branched chain transacylase E2 (DBT) in mouse kidney under hypoxia. Proteome Sci. 2015;13:4.

26. Hauri S, Wepf A, van Drogen A, Varjosalo M, Tapon N, Aebersold R, et al. Interaction proteome of human Hippo signaling: modular control of the co-activator YAP1. Mol Syst Biol. 2013;9:713.

27. Li Z, Weng H, Su R, Weng X, Zuo Z, Li C, et al. FTO Plays an Oncogenic Role in Acute Myeloid Leukemia as a N(6)-Methyladenosine RNA Demethylase. Cancer Cell. 2017;31(1):127-41.

28. Ratnadiwakara M, Anko ML. mRNA Stability Assay Using transcription inhibition by Actinomycin D in Mouse Pluripotent Stem Cells. Bio Protoc. 2018;8(21):e3072.

29. Warrier S, Van der Jeught M, Duggal G, Tilleman L, Sutherland E, Taelman J, et al. Direct comparison of distinct naive pluripotent states in human embryonic stem cells. Nature communications. 2017;8:15055.

30. Miao D, Shi J, Xiong Z, Xiao W, Meng X, Lv Q, et al. As a prognostic biomarker of clear cell renal cell carcinoma RUFY4 predicts immunotherapy responsiveness in a PDL1-related manner. Cancer Cell Int. 2022;22(1):66.

31. Xiong Z, Xiong W, Xiao W, Yuan C, Shi J, Huang Y, et al. NNT-induced tumor cell "slimming" reverses the pro-carcinogenesis effect of HIF2a in tumors. Clin Transl Med. 2021;11(1): e264.

32. Harvey KF, Zhang X, Thomas DM. The Hippo pathway and human cancer. Nat Rev Cancer. 2013;13(4):246-57.

33. Misra JR, Irvine KD. The Hippo Signaling Network and Its Biological Functions. Annu Rev Genet. 2018;52:65-87.

34. Yu FX, Zhao B, Guan KL. Hippo Pathway in Organ Size Control, Tissue Homeostasis, and Cancer. Cell. 2015;163(4):811-28.

35. Wang Y, Xu X, Maglic D, Dill MT, Mojumdar K, Ng PK, et al. Comprehensive Molecular Characterization of the Hippo Signaling Pathway in Cancer. Cell Rep. 2018;25(5):1304-17 e5.

36. He L, Li H, Wu A, Peng Y, Shu G, Yin G. Functions of N6-methyladenosine and its role in cancer. Mol Cancer. 2019;18(1):176.

37. Roundtree IA, Evans ME, Pan T, He C. Dynamic RNA Modifications in Gene Expression Regulation. Cell. 2017;169(7): 1187-200.

38. Zeng C, Huang W, Li Y, Weng H. Roles of METTL3 in cancer: mechanisms and therapeutic targeting. J Hematol Oncol. 2020;13(1):117.

39. Walther TC, Farese RV, Jr. Lipid droplets and cellular lipid metabolism. Annu Rev Biochem. 2012;81:687-714.

40. Zhao B, Ye X, Yu J, Li L, Li W, Li S, et al. TEAD mediates YAP-dependent gene induction and growth control. Genes Dev. 2008;22(14):1962-71.

41. Gerke V, Moss SE. Annexins: from structure to function. Physiol Rev. 2002;82(2):331-71.

42. Shalhout SZ, Yang PY, Grzelak EM, Nutsch K, Shao S, Zambaldo C, et al. YAP-dependent proliferation by a small molecule targeting annexin A2. Nat Chem Biol. 2021;17(7): 767-75.

43. Grindheim AK, Saraste J, Vedeler A. Protein phosphorylation and its role in the regulation of Annexin A2 function. Biochim Biophys Acta Gen Subj. 2017;1861(11 Pt A):2515-29.

44. Zhang C, Zhou T, Chen Z, Yan M, Li B, Lv H, et al. Coupling of Integrin alpha5 to Annexin A2 by Flow Drives Endothelial Activation. Circ Res. 2020;127(8):1074-90.

45. Nazmi AR, Ozorowski G, Pejic M, Whitelegge JP, Gerke V, Luecke H. N-terminal acetylation of annexin A2 is required for S100A10 binding. Biol Chem. 2012;393(10):1141-50.

46. Xiao Y, Thakkar KN, Zhao H, Broughton J, Li Y, Seoane JA, et al. The m(6)A RNA demethylase FTO is a HIF-independent synthetic lethal partner with the VHL tumor suppressor. Proc Natl Acad Sci U S A. 2020;117(35):21441-9.

47. Li T, Hu PS, Zuo Z, Lin JF, Li X, Wu QN, et al. METTL3 facilitates tumor progression via an m(6)A-IGF2BP2-dependent mechanism in colorectal carcinoma. Mol Cancer. 2019;18(1): 112.

48. Huang H, Weng H, Chen J. m(6)A Modification in Coding and Non-coding RNAs: Roles and Therapeutic Implications in Cancer. Cancer Cell. 2020;37(3):270-88.

49. Yang L, Chen Y, Liu N, Lu Y, Ma W, Yang Z, et al. CircMET promotes tumor proliferation by enhancing CDKN2A mRNA decay and upregulating SMAD3. Mol Cancer. 2022;21(1):23.

50. Zhang C, Chen L, Liu Y, Huang J, Liu A, Xu Y, et al. Downregulated METTL14 accumulates BPTF that reinforces super-enhancers and distal lung metastasis via glycolytic reprogramming in renal cell carcinoma. Theranostics. 2021;11(8):3676-93.

51. Sanchez DJ, Simon MC. Genetic and metabolic hallmarks of clear cell renal cell carcinoma. Biochim Biophys Acta Rev Cancer. 2018;1870(1):23-31.

52. Bensaad K, Favaro E, Lewis CA, Peck B, Lord S, Collins JM, et al. Fatty acid uptake and lipid storage induced by HIF-1alpha contribute to cell growth and survival after hypoxia-reoxygenation. Cell Rep. 2014;9(1):349-65.

53. Xiong Z, Xiao W, Bao L, Xiong W, Xiao H, Qu Y, et al. Tumor Cell "Slimming" Regulates Tumor Progression through PLCL1/UCP1-Mediated Lipid Browning. Adv Sci (Weinh). 2019;6(10):1801862.

54. Zhang X, Saarinen AM, Hitosugi T, Wang Z, Wang L, Ho TH, et al. Inhibition of intracellular lipolysis promotes human cancer cell adaptation to hypoxia. Elife. 2017;6:e31132.

55. Cancer Genome Atlas Research N. Comprehensive molecular characterization of clear cell renal cell carcinoma. Nature. 2013;499(7456):43-9.

56. Menendez JA, Lupu R. Fatty acid synthase and the lipogenic phenotype in cancer pathogenesis. Nat Rev Cancer. 2007;7(10):763-77.

57. Wang L, Lin M, Chu M, Liu Y, Ma J, He Y, et al. SPOP promotes ubiquitination and degradation of LATS1 to enhance kidney cancer progression. EBioMedicine. 2020;56:102795.

58. Kim N, Kim S, Lee MW, Jeon HJ, Ryu H, Kim JM, et al. MITF Promotes Cell Growth, Migration and Invasion in Clear Cell Renal Cell Carcinoma by Activating the RhoA/YAP Signal Pathway. Cancers (Basel). 2021;13(12):2920.

59. Elisi GM, Santucci M, D'Arca D, Lauriola A, Marverti G, Losi L, et al. Repurposing of Drugs Targeting YAP-TEAD Functions. Cancers (Basel). 2018;10(9):329.

SUPPORTING INFORMATION

Additional supporting information can be found online in the Supporting Information section at the end of this article.